

## Behaviour of a floc population during a tidal cycle: Laboratory experiments and numerical modelling

Romarc Verney<sup>a,\*</sup>, Robert Lafite<sup>b</sup>, Jean Claude Brun-Cottan<sup>c</sup> and Pierre Le Hir<sup>a</sup>

<sup>a</sup> Ifremer, Laboratoire Dyneco/Physed, BP 70, 29280 Plouzané, France

<sup>b</sup> UMR CNRS 6143 M2C, Université de Rouen, Bat. Irese A, 76821 Mont Saint Aignan Cedex, France

<sup>c</sup> UMR CNRS 6143 M2C, Université de Caen, 21 avenue des Tilleuls, 14000 Caen, France

\* Corresponding author : Romarc Verney, Tel./fax: +33 02 29 00 85 33, email address :

[romarc.verney@ifremer.fr](mailto:romarc.verney@ifremer.fr)

### Abstract:

An approach combining laboratory experiments and numerical modelling was used to investigate the behaviour of a floc population during an idealized tidal cycle. The experiment was conducted on suspended sediments at a concentration of  $93 \text{ mg l}^{-1}$  collected in the field. It was based on a jar test device to reproduce tidal-induced turbulence and coupled with a CCD camera system and image post-processing software to monitor floc size distribution. At the same time, a 0D size-class based aggregation/fragmentation model (FLOCMOD) was developed to simulate changes in the floc population over the tidal cycle. Experimental results revealed strong variability of the behaviour of microfloc and macrofloc populations with respect to the varying shear rates observed *in situ*. In particular, the major dependency of floc sizes on the Kolmogorov microscale was confirmed. Time-scale differences were also observed for aggregation and fragmentation processes which led to asymmetrical floc behaviour despite symmetrical tidal forcing. Model results, i.e. average diameter, maximum diameter and floc size distribution, were in good agreement with experimental data with an RMS error between observed and computed average diameters of below  $25 \mu\text{m}$  over the tidal cycle. FLOCMOD was optimized in terms of the time step, number of size classes and size range: only seven classes ranging from  $50$  to  $643 \mu\text{m}$  associated with a dynamically-adaptable time step were needed to correctly reproduce experimental results, characterized by an RMS error of less than  $5 \mu\text{m}$  with respect to the reference case (100 classes from  $4$  to  $1500 \mu\text{m}$ ). Sensitivity analyses were performed on major parameters or processes: initial floc size distribution, primary particle size, fractal dimension and fragmentation function (binary, ternary, erosion or collision-induced fragmentation). Results showed that initial floc size distribution played a role only during the first aggregation stage. Low variability of the fractal dimension did not significantly modify model results, while larger differences were observed when the primary particle size was changed, especially towards the largest sizes ( $10 \mu\text{m}$ ). Nevertheless, these two structural parameters had a strong impact on the calculated mean settling velocity with differences of  $0.2 \text{ mm s}^{-1}$  compared with the reference case. Different fragmentation functions were shown to significantly modify model results, except for collision-induced shear stress. In particular, combining floc erosion with binary breakup in the shear fragmentation term enabled us to reproduce bimodal distributions, patterns that are typically observed *in situ*.

**Keywords:** Flocculation; Tidal cycle; Laboratory experiment; FLOCMOD; 0D model; Sensitivity analysis; Optimization

## 1 Introduction

Aggregation and fragmentation are key processes in investigating cohesive sediment dynamics in natural systems as they control the formation of macroflocs, their size and main structural characteristics, and hence their fate in the water column (Eisma, 1996). These processes are essential in estuarine macrotidal environments as controlling parameters vary strongly over time and space, particularly hydrodynamics and related turbulence, which are reported to be among the most important factors (Milligan and Hill, 1998; Manning and Dyer, 1999).

Many studies have observed and quantified flocculation processes and changes in floc populations over time using *in situ* measurements during tidal cycles (Eisma and Li, 1993; Fennessy et al., 1994; Fennessy and Dyer, 1996; Van der Lee, 2000; Fettweis et al., 2006; Uncles et al., 2006). These authors observed major changes in floc populations during the different stages of the tidal cycle, and a strong dependency on hydrodynamic conditions, often quantified by shear rate,  $G$ , or the Kolmogorov microscale,  $\eta$ . However, most of these measurements were based on Eulerian sampling. This does not enable the behaviour of a population of flocs to be monitored with respect to the forcings they undergo when transported within the system but only particles flowing through the sampling volume with no knowledge of their previous history. However, aggregation processes are complex mechanisms that last from several minutes to several hours depending on the nature of SPM (van Leussen, 1994), and information on their history is thus essential to understand floc behaviour.

Numerical modelling studies complement *in situ* measurements and provide full knowledge of floc behaviour in a natural system. Two or three-dimensional hydrodynamic and sediment transport models are required, coupled with a process-based flocculation model. Three main flocculation models of decreasing complexity are described in the literature: i) size-class based models (SCB) (Krishnappan, 1991; McAnally and Mehta, 2001,2002 ; Maggi et al., 2007; Xu et al., 2008), ii) distribution-based models (Maerz et al., submitted) and iii) a simplified model based on changes in a characteristic diameter over time (Winterwerp, 2002). Computation of the third model is fast (only one class simulated) but it only provides limited information on the floc population, and although suitable for operational issues, it is too simple to investigate the behaviour of the floc population. The distribution-based model is rapid to compute and provides more knowledge on floc size distribution but is limited by the assumption of a fixed distribution: bimodal populations as observed by Benson and French (2007) could not be computed with such distribution-based models. SCB models are the best way to investigate floc behaviour as they provide detailed information on floc populations. However, the SCB models described in the literature are limited by the large number of size classes required to correctly reproduce aggregation/fragmentation processes and their computation costs are thus high. This explains why they have not yet been coupled with hydrodynamic and sediment transport models.

The objective of the present study is to investigate floc behaviour under an idealized hydrodynamic tidal forcing, combining laboratory experiment and SCB model simulations.

The laboratory experiment provided controlled and homogeneous hydrodynamic conditions and observation of a population of flocs, which were then computed with a SCB model. This approach is based on the assumption that no flocs either settle or are advected, and that the concentration thus remains constant. This is a simplified approach compared with the complex 3D floc behaviour observed in nature but provides key information on aggregation/fragmentation processes and their modelling. The present study investigated the capacity of a size-class based model to reproduce experimental results, its possible optimization for future use in a 1DV, 2D or 3D models, and its sensitivity to key parameters such as structural parameters and fragmentation functions. This study can be considered as an intermediate step before investigating the fate of flocs populations in natural systems.

## 2 Experimental setup

A laboratory experiment was conducted in 2005 to investigate the behaviour of a population of flocs during an idealized tidal cycle considering one the main controlling parameter of flocculation processes, turbulence. A 'video in lab' (VIL) device was used in this study both to observe floc populations and to artificially reproduce variations in shear rate at the tidal scale, as observed in the field above intertidal mudflats (Van der Lee, 1998; Verney et al., 2009). This device consists of a small (13 cm wide, 20 cm high) cylindrical test chamber equipped with a ten-speed impeller to control turbulent agitation. The turbulent field generated inside the test chamber was calibrated from turbulent kinetic energy measurements performed with a laser Doppler velocimeter (Verney, 2006). Results confirmed homogeneous shear rates inside the cylinder for all impeller rotation speeds (corresponding to equivalent shear rates of from 0 to 12 s<sup>-1</sup>). Subsequently, aggregates within the whole test chamber were thus assumed to undergo a unique shear stress at a given time thus making the experiment suitable for OD model comparison.

Floc size distributions were obtained from floc image recording and post processing. The post-processing method used to obtain floc size distribution is briefly described hereafter but a full description can be found in Verney et al. (2009). The 'video in lab' was equipped with a Sony CCD camera and lens that provide 8 μm pixel resolution images for the maximum enlargement. A backlight was placed opposite the CCD camera to provide a uniform white background upon which flocs appear as greyscale silhouettes. Particle separation is automatically processed by the ELLIX® software (Microvision®), which uses image thresholding to detect particles larger than 50 μm. Below this limit, the pixel resolution of the floc measurements is not consistent and hence the smallest microflocs are not accounted for in the description of the floc population during the experiment. Separation results were individually checked to remove detection errors. Floc sizes are expressed as a surface equivalent diameter, calculated as the diameter of the sphere with a projected area (A) equal to the detected particle area (Billiones et al., 1999; Flory et al., 2004; Verney et al., 2009) such as

$$D = \sqrt{\frac{4A}{\pi}} \quad (\text{Eq. 1})$$

In addition to the characteristic size, floc length (L) and circularity (C) were estimated. L is the length of the larger axis of the ellipse inscribing the floc area. C is computed as :

$$C = \frac{4\pi A}{P^2} \quad (\text{Eq. 2})$$

where P is the perimeter of the detected floc. Therefore, C=1 for perfect spherical flocs and C→0 for string flocs.

Further in the manuscript, floc size distributions refer to surface distributions. Finally, the characteristic size of a population of particles corresponds to the mean surface diameter (D(i)) weighted with the detected surface area of the floc (A(i)):

$$\langle D \rangle = \frac{\sum_{i=1}^N D(i)A(i)}{\sum_{i=1}^N A(i)} \quad (\text{Eq. 3})$$

An idealized symmetric tidal cycle was reproduced within the test chamber by step-by-step matching of agitation-induced turbulence with field observations, from 0 (complete slack water period) to  $12 \text{ s}^{-1}$  (maximum tidal current imposed in the model, corresponding to values observed above intertidal mudflats in the upper part of the Seine estuary (France), (Verney et al., 2009, Figure 1). Sediments used during the experiment were collected in February 2005 in the upper part of the Seine estuary (freshwater part, muddy sediments). Their grain size distribution was analyzed with a Coulter Counter, and showed that the collected suspended sediments were muddy with a median size around  $10 \mu\text{m}$ . According to measurements carried out in the area during winter by Verney et al. (2009), no peaks corresponding to diatom blooms were observed and the organic matter content was estimated around 5%. Sediments were directly introduced in the test chamber without any treatment at a concentration of  $93 \text{ mg l}^{-1}$ , and deflocculated by high turbulence mixing to reach the initial condition of the tidal test.

### 3 Model description (FLOCMOD)

#### 3.1 Floc characteristics and size distribution

FLOCMOD is the size-class-based (SCB) model used to reproduce the flocculation and fragmentation processes. The SCB model is based on the population equation system originally proposed by Smoluchowski (1917), which described the floc population in  $N$  discrete classes. In previous modelling studies, particles were assumed to behave as full spheres and were characterized by their equivalent diameter. *In situ* floc measurements demonstrated that the density of flocs is variable and floc structure and density have to be included in numerical approaches. In the present study, following Kranenburg (1994), the fractal behaviour of flocs was assumed to be the main floc characteristic sizes in each class  $i$  (diameter  $D_i$ , mass  $m_i$  and density  $\rho_{f,i}$ ) and can be expressed via the fractal dimension  $n_f$ : (Figure 2)

$$m_i = \rho_s \frac{\pi}{6} D_p^3 \left( \frac{D_i}{D_p} \right)^{n_f} \quad (\text{Eq. 4})$$

$$\rho_{f,i} = \rho + (\rho_s - \rho) \left( \frac{D_p}{D_i} \right)^{3-n_f} \quad (\text{Eq. 5})$$

The number of size classes required for SCB models depends on their structure. Three methods are available. A first group of models (Lagrangian) uses as many classes as created particles (Maggi et al., 2007). This can yield hundreds of classes and may lead to high computation costs when integrated in 2D/3D models. A second group uses size classes defined by mean sizes (or mean masses) and lower and upper boundaries. This method requires to ensure particle growth continuity regarding the size class distribution, i.e. that the mass corresponding to the lower boundary of the size class  $i$  is smaller than twice the mass of the class  $i-1$  (McAnally and Mehta, 2001). This allows the number of size classes to be reduced. In order to optimize the number of size classes required to realistically reproduce flocculation processes, a mass interpolation scheme is applied in FLOCMOD (Xu et al., 2008) for aggregation and fragmentation. Each class corresponds to a typical floc size, logarithmically distributed from the primary particle diameter  $D_p$  to the maximum floc size  $D_{\max}$  and boundaries between these classes are ignored. Therefore, the mass of each newly formed floc (from aggregation or fragmentation) is mass-linearly distributed into the two neighbour classes (see Fig. 3). This means that not as many classes have to be included as potentially newly formed flocs, and mass continuity is ensured. The number of size classes can be changed depending on the required size range  $[D_{\min} D_{\max}]$ .

#### 3.2 Flocculation processes

Particle exchanges between classes are allowed through processes limited to two-body interactions (McAnally and Mehta, 2001) and governed by aggregation, shear breakup and collision breakup terms

(both for gain and loss of particles) as described hereafter in the generic equation, where  $n_k$  is the number of particles in the  $k$  class (in  $m^{-3}$ ):

$$\frac{dn_k}{dt} = G_{aggr}(k) + G_{break\_shear}(k) + G_{break\_coll}(k) - L_{aggr}(k) - L_{break\_shear}(k) - L_{break\_coll}(k) \quad (Eq. 6)$$

### 3.2.1 Aggregation ( $G_{aggr}$ and $L_{aggr}$ )

These terms correspond to the gain or loss of class  $k$  particles when i) two particles collide and ii) the collision is efficient, i.e. the newly formed bound between the two particles can withstand the shear induced by the collision. In the present study (0D), shear aggregation is assumed to be dominant and differential settling aggregation is neglected. Therefore, the two-body collision probability function  $A(i,j)$  is a function of the shear rate  $G$  and particle diameters  $D_i$  and  $D_j$  (McAnally and Mehta, 2001,2002; Thomas et al., 1999):

$$G_{aggr}(k) = \frac{1}{2} \sum_{i+j=k} \alpha_{ij} A(i,j) n_i n_j \quad (Eq. 7)$$

$$L_{aggr}(k) = \sum_{i=1}^N \alpha_{ik} A(i,k) n_i n_k \quad (Eq. 8)$$

$$A(i,j) = \frac{1}{6} G (D_i + D_j)^3 \quad (Eq. 9)$$

The collision efficiency  $\alpha_{ij}$  represents particle cohesiveness, i.e. physico-chemical forces and the sticking properties of organic matter. A few studies investigated flocculation efficiency and reported a generic mathematical description/formulation of  $\alpha_{ij}$  (Friedlander, 1977; McAnally and Mehta, 2001; Maggi et al., 2007). However, few is known about the physico-chemical properties of our sediment. Consequently in the present study,  $\alpha_{ij}$  is set as a constant value ( $\alpha$ ) independent of the floc size and used as an optimization parameter in combination with the fragmentation rate  $\beta_i$  (see below).

### 3.2.2 Shear breakup ( $G_{break\_shear}$ and $L_{break\_shear}$ )

These terms represent the gain and loss of  $k$ -class particles from the fragmentation of larger flocs ( $i \geq k$ ) induced by the turbulent shear stress. The probability of a  $k$ -class floc to break up for a given  $G$  value is expressed by the fragmentation probability function  $B_i$  as proposed by (Winterwerp, 2002).

$$G_{break\_shear}(k) = \sum_{i=k+1}^N FDBS_{ki} B_i n_i \quad (Eq. 10)$$

$$L_{break\_shear}(k) = B_k n_k \quad (Eq. 11)$$

$$B_i = \beta_i G^{\beta_2} D_i \left( \frac{D_i - D_p}{D_p} \right)^{\beta_3} \quad (\text{Eq. 12})$$

where  $\beta_1$  is the fragmentation rate, as a function of floc yield strength, which depends on the physico-chemical properties of the floc and on organic matter content, similarly to  $\alpha$ . As mentioned above,  $\alpha_{ij}$  and  $\beta_i$  are used as optimization parameters, and are independent of floc size:  $\beta_i = \beta$ .

Following Winterwerp's assumption between equilibrium floc size and the Kolmogorov microscale,  $\beta_2$  is fixed to 3/2 and  $\beta_3 = 3 - n_f$  (Winterwerp, 2002).

$FDBS_{ij}$  is the distribution function of fragmented flocs for shear breakup. Knowledge of break-up modes is poor and mainly based on theoretical investigations as reported in Maggi (2005). Faced with this uncertainty, various fragmentation distribution functions can be tested to analyse their influence on floc population dynamics:

- i) Binary distribution, i.e. the fragmentation of a  $m_i$ -mass particle in two particles of equivalent mass  $m_i/2$

$$FDBS_{ij} = \begin{cases} 2 & \text{if } m_j = \frac{m_i}{2} \\ 0 & \text{otherwise} \end{cases} \quad (\text{Eq. 13})$$

- ii) Ternary distribution, i.e. the fragmentation of a  $m_i$ -mass particle in one particle of mass  $m_i/2$  and two particles of equivalent mass  $m_i/4$

$$FDBS_{ij} = \begin{cases} 1 & \text{if } m_j = \frac{m_i}{2} \\ 2 & \text{if } m_j = \frac{m_i}{4} \\ 0 & \text{otherwise} \end{cases} \quad (\text{Eq. 14})$$

- iii) Erosion, i.e. the fragmentation of a  $m_i$ -mass particle in one large fragment and several ( $k$ ) small fragments of the same mass  $m_k$  (Hill, 1996).

$$FDBS_{ij} = \begin{cases} 1 & \text{if } m_j = m_i - k * m_k \\ k & \text{if } m_j = m_k \\ 0 & \text{otherwise} \end{cases} \quad (\text{Eq. 15})$$

### 3.2.3 Collision-induced break-up ( $G_{\text{break\_coll}}$ and $L_{\text{break\_coll}}$ )

Two-floc collisions can lead to aggregation (§ 3.2.1) but also to break-up if the collision-induced shear stress ( $\tau^{coll}$ ) experienced by the particles exceeds the strength ( $\tau_y$ ) of at least one of the two colliding particles. Gain and loss terms of collision-induced break-up ( $G_{break\_coll}$  and  $L_{break\_coll}$ ) are defined as proposed by McAnally and Mehta (2001) similarly to the shear aggregation terms  $G_{aggr}(k)$  and  $L_{aggr}(k)$ :

$$G_{break\_coll}(k) = \sum_{i,j} FDBC_{ij} A(i,j) n_i n_j \quad (Eq. 16)$$

$$L_{break\_coll}(k) = \sum_{i=1}^N FDBC_{ik} A(i,k) n_i n_k \quad (Eq. 17)$$

Where  $A(i,j)$  is still the collision probability function of two flocs  $i$  and  $j$ . The collision-induced fragmentation distribution function  $FDBC_{ij}$  determines i) if fragmentation occurs, i.e. if the collision-induced shear stress ( $\tau^{coll}$ ) experienced by the particles exceeds the strength ( $\tau_y$ ) of at least one of the two colliding particles and ii) how floc fragments are distributed. Calculating  $FDBC_{ij}$  requires first to determine  $\tau^{coll}$  and  $\tau_y$ .

The collision-induced shear stress undergone by a floc  $i$  from its collision with a floc  $j$  ( $\tau_{ij,i}^{coll}$ ) is expressed by:

$$\tau_{ij,i}^{coll} = \frac{8 \left( \frac{G(D_i + D_j)}{2} \right)^2 m_i m_j}{\pi F_p D_i^2 (D_i + D_j) (m_i + m_j)} \quad (Eq. 18)$$

While the strength of the floc  $i$  ( $\tau_{y,i}$ ) is estimated from floc density (itself related to floc size):

$$\tau_{y,i} = F_y \left( \frac{\Delta \rho_i}{\rho} \right)^{\frac{2}{3-n_f}} \quad (Eq. 19)$$

$F_p$  represents the relative depth of interparticle penetration and is estimated to be 0.1 (Krone, 1963; McAnally, 1999; McAnally and Mehta, 2001).  $F_y$  represents the yield strength. Estimation of this parameter is highly empirical and a constant value of  $O\{10^{-10}\}$  N is used hereafter as proposed by (Winterwerp, 2002).

For two-body interactions (flocs  $i$  and  $j$ ), two types of failures are likely to happen and control the expression of collision-induced fragmentation distribution function  $FDBC_{ij}$  (McAnally, 1999; McAnally and Mehta, 2001):

- i)  $\tau_{y,i} > \tau_{ij,i}^{coll}$  and  $\tau_{ij,j}^{coll} > \tau_{y,j}$ : The collision-induced shear stress exceeds the shear strength of the weakest aggregate only, consequently, during the collision, the  $j$  particle breaks into two fragments ( $F_{j,1}$  and  $F_{j,2}$ ) such as  $m_{F_{j,1}}=13/16m_j$  and  $m_{F_{j,2}}=3/16m_j$ .  $F_{j,1}$  is a free fragment while  $F_{j,2}$  is bound with the  $i$  particle.

- ii)  $\tau_{ij,i}^{coll} > \tau_{y,i}$  and  $\tau_{ij,j}^{coll} > \tau_{y,j}$ : The shear stress is larger than shear strength of both i and j particles. Both particles break into two fragments ( $F_{i,1}$ ;  $F_{i,2}$ ) and ( $F_{j,1}$ ;  $F_{j,2}$ ) such as  $[m_{F_{i,1}}; m_{F_{i,2}}] = 13/16 [m_i; m_i]$  and  $[m_{F_{j,1}}; m_{F_{j,2}}] = 3/16 [m_j; m_j]$ . Two particles are formed from the two primary particles  $F_{i,1}$  and  $F_{j,1}$ . A third particle is formed from the two fragments ( $F_{i,2}$  and  $F_{j,2}$ ) that bound during collision.

### 3.2.4 Time step

An explicit integration scheme was adopted to solve the aggregation/fragmentation equations such as Eq. 6 can be written as:

$$N_k^{t+1} = N_k^t + \Delta t * (G_{aggr}(k) + G_{break\_shear}(k) + G_{break\_coll}(k) - L_{aggr}(k) - L_{break\_shear}(k) - L_{break\_coll}(k)) \quad (Eq. 20)$$

Aggregation and fragmentation occur simultaneously for all size classes and careful attention must be paid to the time step used to ensure mass conservation and that all classes do not receive a negative number of particles. In this case, two options are available:

- i) a constant time step, which must be small, i.e. equal or lower than 1 s;
- ii) a varying time step, which prevents more particles aggregating or fragmenting than exist in each class;

The latter option is the most attractive as it can significantly reduce computational costs. At every time step, a first calculation of the mass of particles exchanged is computed with the preceding time step. If at least one class has a negative mass, aggregation/fragmentation are re-processed with a new time step that is half the previous one until all masses are positive after aggregation/fragmentation calculation. Similarly, if all masses are positive, calculations are made with a new time step that is twice the previous one, until one of the size classes have negative mass or that  $\Delta t$  reached a maximum time step fixed to 60s.

## 4 Results

### 4.1 Experimental results

Results of the laboratory simulation of a tidal cycle are shown in Figure 4. They are represented as time series of i) the Kolmogorov microscale (minimum and average values), ii) the mean diameter  $D$  with its standard deviation (vertical bars), iii) the maximum observed diameter  $D_{max}$ , iv) the maximum floc length  $L_{max}$ . The behaviour of the floc population was examined during different stages of the tidal

cycle: low flood current - slack water period (low water), flood current acceleration period, flood current deceleration period, low flood current-slack –low ebb current period (high water), ebb current acceleration period, ebb current deceleration period.

The first slack period (Figure 4 - I) corresponded to a two-hour period at low shear rate ( $G = 1 \text{ s}^{-1}$ ).

During this period, aggregation dominated and the mean floc size grew steadily from  $65 \mu\text{m}$  to  $266 \mu\text{m}$ . Just before the flood ( $t = 120 \text{ min}$ ), the maximum floc diameter observed was  $365 \mu\text{m}$ . During the flood current acceleration phase (Figure 4 - II), the shear rate increased and promoted fragmentation that induced an abrupt decrease in  $D$  and  $D_{\text{max}}$ . When flood currents were the largest,  $D$  was smaller than  $70 \mu\text{m}$  and  $D_{\text{max}}$  close to  $90 \mu\text{m}$ , which denotes a narrow distribution. Next shear stress decreased when flood currents decreased (Figure 4 - III): aggregation progressively counterbalanced fragmentation and  $D$  and  $D_{\text{max}}$  increased to reach values of  $120 \mu\text{m}$  and more than  $220 \mu\text{m}$  respectively at  $t=270 \text{ min}$ .

Slack period corresponded to  $G$  values equal or below  $1 \text{ s}^{-1}$  (Figure 4 - IV). During this phase, aggregation was strong, and  $D$  reached values close to  $250 \mu\text{m}$  at  $t=360 \text{ min}$ . It should be noted that, just before complete slack water (Figure 4 – IV), the  $D_{\text{max}}$  value was not consistent with previous values. This discrepancy was possibly due to an error in particle detection. During complete slack (Figure 4 - V), agitation was stopped,  $G=0 \text{ s}^{-1}$ , and flocs settled rapidly:  $D$  dropped from  $250 \mu\text{m}$  to  $170 \mu\text{m}$  after two minutes and was  $70 \mu\text{m}$  after 30 min. Next, the current slowly increased (Figure 4 - VI), which was simulated by a 90 min period at  $G=1 \text{ s}^{-1}$ . Agitation rerun induced floc resuspension, and  $D$  and  $D_{\text{max}}$  increased to  $220 \mu\text{m}$  and  $360 \mu\text{m}$  respectively. These values were similar to the characteristic floc sizes observed before settling. The flocculation state was stable throughout the slack period: after 90 min,  $D$  was  $217 \mu\text{m}$  and  $D_{\text{max}}$  was  $355 \mu\text{m}$ . Next, similarly to the flood phase, the largest flocs underwent enhanced fragmentation during the ebb acceleration phase (Figure 4 – VII), and  $D$  and  $D_{\text{max}}$  decreased rapidly to  $80 \mu\text{m}$  and  $105 \mu\text{m}$  respectively for maximum tidal current. During the decelerating phase (Figure 4 – VIII), aggregation again dominated, and the mean and maximum floc size were  $150 \mu\text{m}$  and  $250 \mu\text{m}$  respectively, at  $t=660 \text{ min}$  and  $G=2 \text{ s}^{-1}$ .

Similarly to other characteristic floc sizes, maximum floc length  $L_{\text{max}}$  was negatively correlated with shear rate, i.e. with increasing values during decreasing or low shear rate periods, and otherwise decreased during high shear rate periods. Comparing floc size time series and Kolmogorov microscale time series demonstrated the dominant influence of turbulence scales on flocculation dynamics: shear rate controls the balance between aggregation and fragmentation processes and therefore a variation in  $G$  causes an inverse change in floc population behaviour. Moreover, maximum floc length never exceeded the mean Kolmogorov microscale, especially during fragmentation stages, underlining the limitation of maximum floc length by the turbulent microscale.

Examination of floc size dynamics also revealed a clockwise hysteresis (Figures 4 and 5). This is caused by the differences between aggregation and fragmentation time scales (time scale is defined as the time required for the floc population to reach a new equilibrium). Whereas shear forcing was exactly symmetrical during accelerating and decelerating phases, during these two stages, floc

population behaviour differed significantly. On one hand, fragmentation dominated during flow acceleration periods (both ebb and flood). This is a rapid process that quasi instantaneously disrupts flocs due to shear fragmentation and collision between flocs. Moreover, shear fragmentation was complete for flocs larger than the Kolmogorov microscale. Figures 4 and 5 show this process during accelerating stages: every shear rate increase broke flocs and the observed maximum floc length rapidly dropped to the Kolmogorov microscale (in  $\sim 1$  min). On the other hand, aggregation was promoted with decreasing shear rates, and was dominant for low  $G$  values ( $\leq 1 \text{ s}^{-1}$ ). However, favourable hydrodynamic conditions do not instantaneously promote floc growth, as aggregation processes also depend on collision rates between different particles, and on collision efficiency. During all aggregation stages reproduced in the experiment, the equilibrium was only reached for  $G$  values of  $1 \text{ s}^{-1}$  after 60 to 100 min. For other shear rate conditions, equilibrium was never reached before the end of every step, which means that the aggregation time scale for these  $G$  values was longer than 20 min.

The experiment simulated one tide cycle with symmetric ebb and flood stages. Hence the behaviour of the floc population could be compared during the two stages (Figure 5b). Results showed that  $D$  (mean and standard deviation values) and  $D_{\max}$  were correctly superimposed for both aggregation and fragmentation dominating periods. This illustrates the reproducibility and redundancy of floc population dynamics for identical shear forcing patterns.

The behaviour of the floc population was also investigated in terms of mean floc circularity (Figure 6). Similarly to other floc characteristics, circularity was strongly dependent on turbulence and in this case positively correlated with shear rate.  $C$  ranged from 0.84, which corresponded to microflocs as observed during settling when only microflocs were in suspension and high shear rate periods; to 0.68, which is characteristic of a macrofloc population. Contrary to floc diameter, circularity differed significantly before and after settling with higher values after deposition and resuspension. This result means that floc structure may have changed during this stage, with the formation of denser particles when flocs settle and collide near the bed. If confirmed by further investigations, this would induce changes in the fractal dimension to be accounted for.

## 4.2 Model results

A reference model configuration was used to compare experimental and model results: i) shear aggregation ii) shear fragmentation only, iii) varying time step, iv) 100 size classes, v)  $n_f=1.9$  (as previously estimated by Verney et al. (2009) on similar experiments) and vi) size range from 4 to 1500  $\mu\text{m}$ . The best results (compared to observation) were obtained for  $\alpha=0.35$  and  $\beta=0.12$ . Results are first discussed in terms of average diameter and second in terms of floc distribution. The initial model condition is the suspended sediment grain size distribution obtained from Coulter Counter analyses. In order to compare the same characteristic sizes, the mean diameter from model results  $D_{\text{mod}}$  was

calculated in exactly the same way as the experimental diameter, i.e. weighted by the projected surface. Moreover, as the lower limit of the 'video in lab' floc size is 50  $\mu\text{m}$ ,  $D_{\text{mod}}$  was calculated over a truncated distribution, from 50 to 1500  $\mu\text{m}$ . Finally, the settling period (380 min < t < 420 min) was excluded from the dataset for model performances analysis (root mean square error (ERMS) calculation), as this process is not simulated in the model.

#### 4.2.1 Average and maximum diameter

The first level of investigation of model performance was to compare time series of experimental and model diameters (both average and maximum) (Figure 7). The maximum computed diameter  $D_{\text{max\_mod}}$  was evaluated as the percentile 90. Results showed that the model correctly reproduced the dynamics of the mean floc diameter, with a RMS value of 24  $\mu\text{m}$  over the 43 experimental data points. Similarly, the  $D_{\text{max\_mod}}$  is in good agreement with the maximum diameter observed experimentally. Moreover, the simulated characteristic time scales of aggregation and fragmentation processes are in good agreement with experimental time scales, i.e. fast fragmentation and slow aggregation.

However, three remarks can be made:

- i) The first flocculation phase (t < 120 min) is not reproduced by the model, whatever the value given to the flocculation efficiency coefficient  $\alpha$ , unlike the two following aggregation stages. This is mainly due to the initial floc size distribution. This aspect is examined in the discussion section.
- ii) During the two following flocculation stages, simulated aggregation starts earlier than observed aggregation
- iii) Settling during complete slack is not reproduced by the model, as particle deposition is not allowed in the 0D model.

#### 4.2.2 Floc size distribution

The time series of the computed floc size distribution (Figures 8 and 9) was in good agreement with experimental data except during the first 120 min and during the settling phase as explained in the previous section. Some differences were observed in floc size distribution during intense flocculation phases ( $G=1 \text{ s}^{-1}$  and  $3 \text{ s}^{-1}$  - Figure 9C/D and 9H). In particular, the model floc size distribution was more significantly widespread towards the largest size classes than in experimental results (except in Figure 9G). This could be explained i) by numerical diffusion, ii) by the absence of other fragmentation sources, such as collision-induced fragmentation, or iii) due to the parameterisation of the shear fragmentation. This point will be discussed in the next section. Nevertheless, the differences in terms of floc behaviour observed experimentally during the tidal phases are well reproduced (Figure 9):

- i) computed distributions are similar for maximum ebb and flood current (Figure 9A and 9E) when floc populations were mainly deflocculated as both peak diameter and distribution were in good agreement
- ii) differences observed for a given shear rate depending that this shear rate corresponds to an accelerating or decelerating periods are also correctly simulated by the model (Figure 9C and 9G)
- iii) the time-lag required for reaching the steady state during the slack period ( $G=1 \text{ s}^{-1}$ ) is also reproduced by the model (Figure 9D and 9H)

Moreover, the model correctly reproduced the clockwise hysteresis that characterised the aggregation and fragmentation processes during the tidal cycle (Figure 10).

## 5 Discussion

### 5.1 Experimental simulation

The mean floc diameter range obtained during the laboratory experiment (Figure 4) was comparable to *in situ* measurements carried out for similar hydrodynamic conditions and sediment concentrations. Eisma and Li (1993) found mean floc sizes between 50  $\mu\text{m}$  and 200  $\mu\text{m}$  and maximum floc size from 200  $\mu\text{m}$  to 600  $\mu\text{m}$  and the largest flocs were observed during slack water periods while experimental results showed that the maximum diameter ranged from 100  $\mu\text{m}$  during high current speed periods to 400  $\mu\text{m}$  during slack water. Moreover, the good agreement of floc size time series during the two tidal stages confirmed the reliability of the 'video in lab' and the reproducibility of the experimental measurements.

According to *in situ* measurements carried out by Fettweis et al. (2006), maximum and mean floc sizes are positively correlated with the Kolmogorov microscale (Figure 4). Our experimental results also highlighted different time scales for aggregation and fragmentation processes. This result confirms results from Winterwerp (2002). On one hand, flocs were quasi-instantaneously disrupted to reach the new equilibrium size when the shear rate increased (the Kolmogorov microscale decreased) because fragmentation is a rapid process. On the other hand, aggregation is a far slower process than fragmentation. Hence a decrease in the shear rate (i.e. an increase of the Kolmogorov microscale) did not lead to rapid particle aggregation and larger floc size and the time required to reach the new equilibrium size was estimated larger than 20 min. These differences in processes time scales are crucial when estimating settling fluxes

### 5.2 Model performances and optimisation

Three main model parameters can dramatically influence computation performances: the number of size classes (N) used to describe the floc population, the size range, and the time step ( $\Delta t$ ). Results are discussed in terms of i)  $D_{\text{mod}}$  RMS error (ERMS) with the N = 100 (A1) test as reference case and ii) computation time  $t_c$  for the period  $t > 200$  min corresponding to peak flood shear rate (Table I).

### 5.2.1 Number of size classes and size range

The size range and the number of size classes are essential as they control the number of particle classes that will be integrated in the 1DV or 3D models. The challenge is to optimize these parameters without changing model results.

In the first step, model results are compared for different number of size classes (N) for the constant size range [4  $\mu\text{m}$ ; 1500  $\mu\text{m}$ ]: 100 (considered as the reference case), 50, 20, 15, and 10 (Figure 11 and Table I). Model results are comparable for N values from 100 to 15, with ERMS from 3 to 9  $\mu\text{m}$ . With N = 10, the size class resolution is too low to correctly reproduce the tidal dynamics (ERMS=60  $\mu\text{m}$ ). Optimization of N leads to a reduction in i) calculation time of aggregation/fragmentation kernels and ii) model run from 257 s to 13 s for a 12-hour simulation period.

The second optimization step consists in reducing the size range and optimizing the number of classes once again. Two methods were tested: recalculating a new size class distribution with different upper ( $D_{\text{max}}$ ) and lower ( $D_{\text{min}}$ ) limit sizes or truncating the size class distribution obtained for 15 classes from 4  $\mu\text{m}$  to 1500  $\mu\text{m}$ . In the present case, D was mainly over 50  $\mu\text{m}$  throughout the tidal cycle and the observed maximum diameter  $D_{\text{max}}$  was smaller than 800  $\mu\text{m}$ .

i) Tests were made with a new size range of [4  $\mu\text{m}$ , 800  $\mu\text{m}$ ] for different numbers of size classes (Figure 11). Results are given in Table I (B.1 to B.6) and presents ERMS and computation time.

Optimizing size range means reducing N down to 14 classes only in the range [4  $\mu\text{m}$ , 800  $\mu\text{m}$ ].

ii) Truncating the original size class distribution (Figure 11 and Table I, A.5.2, A.5.3, A.5.4) enabled reduction of the number of size classes down to 7 on the range [50  $\mu\text{m}$ , 643  $\mu\text{m}$ ] and computation time to 5.6 s while ERMS remained below 5  $\mu\text{m}$ .

Truncating the size class distribution was shown to provide the best model performances in terms of the number of size classes, computation time, and RMS error compared with the reference case A1. This method should be preferred if advanced optimization is required.

### 5.2.2 Time step

Time step methods were evaluated by comparing model performances with two configurations (N=15 and size range is [4  $\mu\text{m}$ , 1500  $\mu\text{m}$ ]): a varying time step (over a time range) or a fixed time step (with different  $\Delta t$  values). The fixed time step  $\Delta t$  is related to the shear rate. In the experimental study, G values never exceeded  $12 \text{ s}^{-1}$ , therefore a time step of 1 s is acceptable. In this case ( $\Delta t = 1 \text{ s}$ ), computation time ( $t_c$ ) is around 95 s (12 h simulation). For a  $\Delta t$  value of 5 s, negative masses are obtained and the model is no more mass-conservative. The varying time step is in the range [0; 60s]

and enables  $t_c$  to be reduced to 17 s. However, the varying time step method can be optimized once again. The varying time step method consists in searching for the time step in which no classes have negative mass concentrations after flocculation processes. This means that a very small time step can be reached as few classes may have very small negative concentrations. To prevent such cases, a negative concentration threshold can be tolerated. The classes concerned are then forced to null concentrations, while all other classes compensate by lowering their concentration in order to maintain mass conservation. Four tests were conducted with different concentration thresholds: 0.00001, 0.0001, 0.001, 0.01 g l<sup>-1</sup>. For thresholds smaller than 0.0001 g l<sup>-1</sup>, this method allowed  $t_c$  to be reduced from 17 s to 11 s without changing the model results (ERMS difference was below 1 µm). In this case, the time step was never below 2 s while it reached 0.1 s when any negative masses were tolerated. For a mass threshold value of 0.001 g l<sup>-1</sup>, ERMS reached 4.8 µm but the time step was still 2 s, while for larger threshold values, concentration compensations need to be high to respect mass conservation and significantly modified model results.

### 5.3 Uncertainty of initial conditions, processes and sensitivity analysis

Aggregation and fragmentation processes are complex and despite considerable research on these topics, several assumptions have to be made as some processes or parameters are still poorly understood. Sensitivity analyses were performed on key parameters or processes for which uncertainty remains: initial floc size distribution, primary particle size, fractal dimension, fragmentation processes, and the coupled parameters {flocculation efficiency  $\alpha$ ; fragmentation factor  $\beta$ }. Similarly to optimization analyses, sensitivity results are discussed as RMS differences over the period from the flood (stage III, Figure 4) to the ebb (stage VIII, Figure 4) with a reference simulation: variable time step,  $N=15$ ,  $D_p=4$  µm,  $n_f=1.9$ ,  $D_{min}=4$  µm and  $D_{max}=1500$  µm,  $\alpha=0.35$  and  $\beta=0.12$ , binary fragmentation.

#### 5.3.1 Initial floc size distribution

Model results revealed the influence of initial distribution: large discrepancies were observed between model and experimental results in the first aggregation stage. The initial distribution applied was deduced from counter coulter measurements performed on SPM sampled for the laboratory experiments. However, this instrument operates with a strong stirring of the sample volume, which could cause more intense breakup than the largest turbulence applied in the VIL, and therefore shift the floc size distribution towards the smallest particles. A sensitivity analysis was performed on this initial condition to estimate its influence on the behaviour of the model: several distributions were tested by shifting the initial distribution from 1 to 4 classes towards the larger floc sizes (Figure 12). The sensitivity analysis clearly showed the consequences of underestimating the initial peak size of the distribution: for larger initial particle sizes, flocculation onset was faster, and correlated better with experimental data. However, sensitivity to the initial distribution disappears after the first

flocculation/deflocculation event as model results are merged after 200 min. This means that the initial distribution is not crucial for modelling, except when flocculation-only laboratory experiments are simulated. Also, this sensitivity exercise has a physical meaning as it confirms that time scale strongly depends on the distance between the equilibrium state and the initial distribution.

### 5.3.2 Floc structure: the role of primary particles and 3D fractal dimension

Fragmentation kernels are controlled by floc structural features, i.e. primary particle sizes and floc fractal dimension, as described in Eq. 12. Hence these parameters are likely to influence flocculation processes and the equilibrium floc size for a given shear rate.

Primary particles are defined as the basic blocks that constitute all flocs. Due to the fractal assumption, these primary particles are characterized by a single size. Conceptually, this size corresponds to clay clusters, and is often fixed at 4  $\mu\text{m}$ . However, deflocculated grain size analyses performed on natural suspended sediments showed that primary particle size spectra can range from 1 to 30  $\mu\text{m}$  (Fettweis, 2008), especially if diatoms are present in suspension.

Model sensitivity was tested for four typical primary particle sizes ( $D_p$ ) observed in nature: 2  $\mu\text{m}$ , 4  $\mu\text{m}$ , 8  $\mu\text{m}$  and 15  $\mu\text{m}$ . The last primary particle size generally corresponds to organic material, such as diatom cells, which should therefore be characterized by small densities. However in the present case, only grain size is investigated and a density of 2600  $\text{kg m}^{-3}$  is assumed for every primary particle size. The objective of the following tests is to examine the numerical sensitivity of the model to small variations of few key parameters. Investigating the influence of such variations on the global physico-chemical processes is out of the scope of this study.

The fractal behaviour of flocs is the strongest assumption made in FLOCMOD. This approach simplifies floc description and reduces floc characteristics as functions of two parameters: its size and its fractal dimension. All numerical models that are based on this assumption also consider that flocs are self-similar fractals, which means that the fractal dimension does not change with size. However, *in situ* and laboratory measurements did not support this assumption as results showed that floc densities strongly decreased with size, which is not only explained by size variations but also by a change in floc fractal dimension (Maggi, 2005). Moreover, floc fractal dimension calculated from *in situ* measurements varied strongly (typically from 1.6 to 2.3) and uncertainties remain on its accuracy (Fettweis, 2008).

According to (Maggi, 2005; Maggi et al., 2007), four main structural behaviours exist:

- i) Euclidian growth:  $n_f$  equals 3.
- ii) Fully self similar:  $n_f$  is a constant over the size range.

iii) Quasi self similar:  $n_f$  equals 3 for primary particles and then decreases with floc size

$$\text{following a power law function : } n_f = 3 \left( \frac{D}{D_p} \right)^{-0.1}$$

iv) Statistically self similar:  $n_f$  equals 3 for very small particles up to a limit size  $D_l$ . Above this

$$\text{threshold, } n_f \text{ decreases with floc size following a power law function: } n_f = 3 \left( \frac{D}{D_l} \right)^{-0.1}$$

In the present study, only cases ii) and iii) are examined as they are the most likely to happen in nature: *in-situ* measurements demonstrated the impossibility of a fully fractal pattern and case iv) is used to describe a full range of particles from crystals to flocs. In case ii), the sensitivity is investigated as the influence of  $n_f$  variability, i.e. 1.9 +/- 0.1 as observed in nature.

Changing primary particle size and floc fractal dimension influence i) fragmentation kernels as observed by Xu et al. (2008) and ii) the initial floc size number distribution. First, as described in Eq. 5 (see § 3.2.2), smaller  $n_f$  values correspond to lower density flocs, that are therefore more subject to breakup: fragmentation is enhanced and smaller flocs are formed. In contrast, larger  $D_p$  or  $n_f$  values yield denser flocs, more resistant to breakup. Consequently, aggregation is enhanced and larger flocs are created. Second, for a given mass concentration in a given class  $k$ , the number of particles  $N_k$  depends on the floc density  $\rho_k$ . Hence flocs made of smaller primary particles are characterized by lower densities (Eq. 5), which finally increases the number of flocs per class with a similar mass concentration and inversely. Similar consequences are induced by variations in fractal dimension.

Therefore small variations in  $D_p$  or  $n_f$  strongly influence flocculation processes as for example looser flocs correspond i) to more particles in suspension which promote aggregation but also ii) to fragile flocs more subjected to break-up. Figure 13a and figure 13b shows that the effect of  $\{D_p, n_f\}$  on floc size number distribution nearly equilibrates their effect on flocculation : in all cases ERMS is below 20  $\mu\text{m}$ , except for large  $D_p$  values of 10  $\mu\text{m}$  for which ERMS reached 58  $\mu\text{m}$ . This is mainly because flocs are denser if  $D_p=10 \mu\text{m}$  and hence fewer flocs participate to aggregation processes. Therefore more time is required for flocs to aggregate and progressively reach the steady state. This explains the specific dynamics of the mean diameter and the mean settling velocity observed in Figure 13a and Figure 13c for  $D_p$  values of 10  $\mu\text{m}$ . In the case of a size-dependant fractal dimension, ERMS was also reduced to 11  $\mu\text{m}$  (Figure 13b).

As a consequence, sensitivity analyses of floc structural parameters demonstrated the satisfactory stability of FLOCMOD under test conditions: realistic uncertainties of  $D_p$  or  $n_f$  induced low variations in model results except for large  $D_p$  values. However, fragmentation is still a poorly known process and in particular uncertainty remains on the choice of the break-up function  $B_i$ . Maerz et al. (submitted)

performed sensitivity analysis to the fractal dimension also with FLOCMOD but with a different break-up term  $B_i$  close to the formulation proposed by Serra and Casamitjana (1998), described as follows:

$$B_i = \beta_i' G^{\beta_2} D_i^{4-n_f} \quad (\text{Eq. 21})$$

These authors found marked differences in model results for similar low variations in fractal dimensions. This means that model stability is strongly dependent on the fragmentation function and hence careful attention must be paid to its choice (see also § 5.3.3).

#### Consequences on floc settling velocities

Floc settling velocity ( $w_s$ ) can be calculated from the modified Stokes Law (e.g. Van Leussen, 1988) out of the hindered settling domain:

$$w_{s,i} = \frac{g}{18\nu} \left( \frac{\rho_i - \rho_w}{\rho_w} \right) D_i^2 \quad (\text{Eq. 22})$$

Therefore, uncertainties concerning primary particle size or floc fractal dimension can strongly influence floc density and cause major variations in floc settling velocity despite the low influence on the average diameter. Figure 13c highlights the significant influence of small uncertainties of each of these two parameters on the mean settling velocity with variations up to  $\pm 0.2 \text{ mm s}^{-1}$  compared with the reference case ( $w_s = 0.4 \text{ mm s}^{-1}$ ) during the periods of low or intermediate turbulence. Such differences could have a strong impact on settling fluxes and on the fate of SPM in natural systems.

#### 5.3.3 Fragmentation processes

Major uncertainties remain concerning the mechanistic process undergone by flocs during shear fragmentation, and especially the size distribution of daughter flocs after fragmentation. Several distributions have been tested (Mietta et al., 2008), and the three main ones are tested here: binary or ternary distributions and floc erosion (See § 3.2.2). Moreover, a second fragmentation process can be added, i.e collision-induced floc fragmentation (See § 3.2.3). This section investigates the consequences of each of these breakup scenarios.

Ternary breakup function led to the formation of smaller flocs than the binary breakup function and as a consequence, the computed floc size was smaller (up to 40%) than the reference case for the whole simulation period.

The effect of floc erosion in the shear fragmentation term is examined in Figure 14 (see also Table II). Here shear fragmentation was assumed to produce simultaneously i) two particles of equal size (binary break-up - FDBS\_binary, reference case) and ii) a large particle and several fragments, the latter corresponding to small particles (floc erosion - FDBS\_erosion).

$$G_{break\_shear}(k) = \sum_{i=k+1}^N (FDBS\_Binary_{ki} + C_{ero} * FDBS\_Erosion_{ki}) B_i n_i \quad (Eq. 23)$$

FDBS\_Binary and FDBS\_Erosion are the floc distribution after shear break for binary breakup and floc erosion respectively (See §3.2.2) and  $C_{ero}$  is the floc erosion contribution to break up, between 0 (no contribution of erosion) to 1 (as much as erosion as binary break-up).

For these tests, binary break up processes were calculated as previously described; floc erosion was considered as an additional fragmentation process. Several erosion configurations were tested where i) floc erosion was characterized by two numbers of fragments produced after erosion (2 or 10 fragments), ii) two fragment sizes ( $D_{fragm}$ ) were investigated: 4  $\mu m$  (primary particle size) or 9.3  $\mu m$  (typical of microflocs) and iii) floc erosion contribution ( $C_{ero}$ ) was calculated as 20%, 50% or 80% of the shear-fragmented mass (in complement of the binary breakup contribution) (see Table II) :

Results showed that the influence of the number of fragments was significant only if  $D_{fragm}$  was 9.3  $\mu m$  (Figure 14).

The equilibrium between aggregation and fragmentation was weakly modified in favour of fragmentation when the floc erosion increased (Figure 14A): the largest mean floc size decreased down to 190  $\mu m$  for a floc erosion contribution of 80%.

Despite the low influence of floc erosion on mean floc size dynamics, results presented in Figures 15 and 16 show that floc erosion also led to the formation of a bimodal distribution all along the tidal cycle, as observed *in situ* (Manning et al., 2006; Benson and French, 2007). In this case a second mode is observed for the class corresponding to the fragment floc size (i.e.  $D_{fragm} = 9.3 \mu m$ ). This highlights the need to simulate these two shear fragmentation mechanisms, i.e. binary or ternary breakup and floc erosion, in process-based flocculation models.

Collision-induced breakup was the last fragmentation term investigated. Results (not shown) demonstrated that this process had no significant influence on floc size dynamics as all curves were merged together. Collisions between two flocs lead to break-up only if the collision-induced shear stress exceeds floc strength. The collision-induced shear stress / floc strength ratio was examined for three shear rate values (1, 5 and 10  $s^{-1}$ ) (Figure 17). For G values of 1  $s^{-1}$  (respectively 10  $s^{-1}$ ) this ratio was greater than 1 only when particles larger than 650  $\mu m$  (respectively 270  $\mu m$ ) collided. However, no flocs belonging to these classes or above were observed and computed during this period (Figure 8) which explains why collision-induced breakup term was not significant for this test. However, as results could change if floc strength was overestimated, it is not possible to conclude that this mechanism should be neglected. Therefore, further investigations are required to conclude on the relative importance of all these breakup processes.

#### 5.3.4 $\{\alpha; \beta\}$ couples: optimal values

Flocculation efficiency and fragmentation rate govern rate processes respectively for aggregation and break up. They are both of obvious physical significance with respect to the binding forces that can be created between two colliding particles or that can resist shear forces. Few parameterizations exist to relate these parameters to the main physical variables like salinity, organic matter content, or particle mineralogy. Therefore,  $\alpha$  and  $\beta$  were used as calibration parameters to search for optimal calibration. This can be achieved by estimating the RMS error between model and experimental datasets over the period from the flood (stage III, Figure 4) to the ebb (stage VIII, Figure 4) for most probable  $\{ \alpha, \beta \}$  couples, i.e.  $\alpha$  ranging from 0 to 1 and  $\beta$  ranging from 0 to 0.5 (Figure 18A). In the present study, the optimal couple was  $\{0.35; 0.12\}$  (Figure 18), and the fragmentation factor was close to the value used by Winterwerp (2002) to calibrate his model ( $\beta=0.112$ ). However, Figure 18 showed that if flocculation efficiency and fragmentation rates are not explicitly calculated, a wide range  $\{ \alpha, \beta \}$  couples may be chosen to calibrate model results and leading to RMS errors ranging from 20  $\mu\text{m}$  to 25  $\mu\text{m}$  between model and experimental results. As observed by Maerz et al. (submitted),  $\alpha$  and  $\beta$  values control the kinetics of flocculation processes: larger values induce more rapid aggregation and fragmentation. The large range of possible  $\{ \alpha, \beta \}$  couples means that differences in model results induced by the  $\{ \alpha, \beta \}$  variability are smaller than the variability of the experimental measurements during aggregation and fragmentation stages. Therefore, complementary laboratory investigations are required to precisely determine the best couple.

Nevertheless, the distribution of the optimal  $\beta$  for every possible  $\alpha$  value (from 0 to 1) can be examined further (Figure 18C). Results showed that a linear relationship can be found between  $\alpha$  and  $\beta$ :

$$\beta = 0.39 \alpha - 0.02 \quad (R^2=0.99) \quad (\text{Eq. 24})$$

A positive correlation between  $\alpha$  and  $\beta$  was expected as fragmentation must increase if aggregation is stronger in order to reach a similar steady state. Modifying the slope (ratio of  $\alpha$  and  $\beta$ ) will move the equilibrium size, i.e. increasing  $\beta/\alpha$  yields smaller flocs (respectively decreasing  $\beta/\alpha$  yields larger flocs). This is in agreement with the relationship given by Winterwerp (2002) between the equilibrium diameter and  $\{ \alpha, \beta \}$ . Further comparisons of model and experimental or *in-situ* measurements are required to confirm this linear pattern and to examine the variability of the slope for different kinds of suspended particulate matter.

## Conclusion

The behaviour of a floc population during an idealized tidal cycle was investigated from laboratory experiments and successfully computed by numerical modelling. Experimental results confirmed the strong influence of turbulence on flocculation processes as already observed *in situ* and in particular the physical limit of floc size. Results also highlighted the consequences of different time scales for aggregation and fragmentation processes on the asymmetrical dynamics of floc populations despite symmetrical forcing.

The model was found to be weakly sensitive to small variations in initial distribution except during the first aggregation stage. The fractal dimension and primary particle size did not strongly influence the time-evolution of floc size distribution, but significantly changed the average settling velocity with a difference of up to  $0.2 \text{ mm s}^{-1}$ . The choice of the fragmentation function was found to play a significant role in the balance between aggregation and fragmentation but further investigations are required to identify the main mechanisms involved. In particular, a focus should be made on the role of the collision effect on floc break up as the experimented range of shear rate did not allow to conclude on this fragmentation process.

The size-class based model correctly reproduced the experimental results both in terms of characteristic sizes (average diameter, maximum diameter) and floc size distribution. This model was successfully optimized to limit the number of size classes by adjusting the size range and reduce computation time with a variable time step. Only seven classes corresponding to a size range from  $50 \mu\text{m}$  to  $650 \mu\text{m}$  were necessary to accurately reproduce experimental data.

The next stage of the project consists in accounting for aggregation by differential settling and modelling floc behaviour in a 1DV and a 3D model, i.e. for a realistic case study, based on the development and optimization work realized in this study.

## 6 References

- Benson, T. and French, J. R. (2007). InSiPID : a new low-cost instrument for in situ particule size measurements in estuarine and coastal waters. *Journal of Sea Research*: 1-22.
- Billiones, R. G., Tackx, M. L. and Daro, M. H. (1999). The geometric features, shape factors and fractal dimensions of suspended particulate matter in the Scheldt Estuary (Belgium). *Estuarine, Coastal and Shelf Science* 48: 293-305.
- Eisma, D. (1996). Flocculation and deflocculation of suspended matter in estuaries. *Netherlands Journal of Sea Research* 20(2/3): 183-199.
- Eisma, D. and Li, A. (1993). Changes in suspended matter floc size during the tidal cycle in the Dollard estuary. *Netherlands Journal of Sea Research* 31(2): 107-117.
- Fennessy, M. J. and Dyer, K. R. (1996). Floc population characteristics measured with INSSEV during the Elbe estuary intercalibration experiment. *Journal of Sea Research* 36(1/2): 55-62.
- Fennessy, M. J., Dyer, K. R. and Huntley, D. A. (1994). Size and settling velocity distribution of flocs in the Tamar estuary during a tidal cycle. *Netherlands Journal of Sea Research* 28(3-4): 275-282.
- Fettweis, M. (2008). Uncertainty of excess density and settling velocity of mud flocs derived from in situ measurements. *Estuarine, Coastal and Shelf Science* 78(2): 426-436.
- Fettweis, M., Francken, F., Pison, V. and Van den Eynde, D. (2006). Suspended particulate matter dynamics and aggregate sizes in a high turbidity area. *Marine Geology* 235(1-4): 63-74.
- Flory, E. N., Hill, P. S., Milligan, T. G. and Grant, J. (2004). The relationship between floc area and backscatter during a spring phytoplankton bloom. *Deep-Sea Research I* 51: 213-223.
- Friedlander, S. K. (1977). *Smoke, dust and haze : fundamentals of aerosol behavior*. New York, Wiley.
- Hill, P. S. (1996). Sectional and discrete representations of floc breakage in agitated suspensions. *Deep-Sea Research I* 43(5): 679-702.
- Kranenburg, C. (1994). The fractal structure of cohesive sediment aggregates. *Estuarine, Coastal and Shelf Science* 39: 451-460.
- Krishnappan, B. G. (1991). Modelling of cohesive sediment transport. *International Symposium on the transport of suspended sediments and its mathematical modelling*, Florence (Italy).

Krone, R. B. (1963). A study of rheologic properties of estuarial sediments. Technical Bulletin 7. Vicksburgh, MS, USAE Communication on Tidal Hydrodynamics.

Maerz, J., Verney, R., Wirtz, K. and Feudel, U. (Submitted). Modeling flocculation processes : intercomparison of a size class-based model and a distribution based-model. Continental Shelf Research INTERCOH'07 Supplement.

Maggi, F. (2005). Flocculation dynamics of cohesive sediment, PhD Thesis, University of Technology, Delft, 136p

Maggi, F., Mietta, F. and Winterwerp, J. C. (2007). Effect of variable fractal dimension on the floc size distribution of suspended cohesive sediment. *Journal of Hydrology* 343(1-2): 43-55.

Manning, A. J. and Dyer, K. R. (1999). A laboratory examination of floc characteristics with regard to turbulent shearing. *Marine Geology* 160: 147-170.

Manning, A. J., Bass, S. J. and Dyer, K. R. (2006). Floc properties in the turbidity maximum of a mesotidal estuary during neap and spring tidal conditions. *Marine Geology* 235(1-4): 193-211.

McAnally, W. H. (1999). Aggregation and deposition of estuarial fine sediment, University of Florida, 382p

McAnally, W. H. and Mehta, A. J. (2001). Collisional aggregation of fine estuarial sediment. Coastal and estuarine fine sediment processes. McAnally, W. H. and Mehta, A. J., Elsevier: 19-39.

McAnally, W. H. and Mehta, A. J. (2002). Significance of aggregation of fine sediment particles in their deposition. *Estuarine, Coastal and Shelf Science* 54: 643-653.

Mietta, F., Maggi, F. and Winterwerp, J. C. (2008). Sensitivity to breakup functions of a population balance equation for cohesive sediments. Sediment and ecohydraulics, INTERCOH 2005. Kusuda, T., Yamanishi, H., Spearman, J. and Gailani, J. Z., Elsevier B.V.: 275-286.

Milligan, T. G. and Hill, P. S. (1998). A laboratory assessment of the relative importance of turbulence, particle composition, and concentration in limiting maximal floc size and settling behaviour. *Journal of Sea Research* 39: 227-241.

Serra, T. and Casamitjana, X. (1998). Effect of shear and volume fraction on the aggregation and break-up of particle. *American Institute of Chemical Engineers* 44(8): 1724-1730.

Smoluchowski, M. (1917). Versuch einer mathematischen theorie des koagulations-kinetik kolloid losungen. Zeitschrift fur Physikalische Chemie 92: 129-168.

Thomas, D. N., Judd, S. J. and Fawcett, N. (1999). Flocculation modelling : a review. Water Research 33(7): 1579-1592.

Uncles, R. J., Stephens, J. A. and Law, D. J. (2006). Turbidity maximum in the macrotidal, highly turbid Humber Estuary, UK : Floccs, fluid mud, stationary suspensions and tidal bores. Estuarine, Coastal and Shelf Science 67 (1-2): 30-52.

Van der Lee, W. (1998). The impact of fluid shear and suspended sediment concentration on the mud floc size variation in the Dollard estuary, The Netherlands. Sedimentary processes in the Intertidal zone. Black, K. S., Paterson, D. M. and Cramp, A., Geological Survey, London, Special Publications. 139: 187-198.

van Leussen, W. (1988). Aggregation of particles, settling velocity of mud floccs: A review. Physical processes in estuaries. Dronkers, J. and van Leussen, W., Springer Verlag, Berlin: 348-403.

van Leussen, W. (1994). Estuarine macroflocs : their role in fine grained sediment transport, University of Utrecht, 488p

Verney, R. (2006). Processus de contrôle de la dynamique des sédiments cohésifs, Université de Rouen, 325

Verney, R., Lafite, R. and Brun Cottan, J. C. (2009). Flocculation potential of natural estuarine particles: the importance of environmental factors and of the spatial and seasonal variability of suspended particulate matter. Estuaries and Coasts, 32, 678-693.

Winterwerp, J. C. (2002). On the flocculation and settling velocity of estuarine mud. Continental Shelf Research 22: 1339-1360.

Xu, F., Wang, D.-P. and Riemer, N. (2008). Modeling flocculation processes of fine-grained particles using a size-resolved method: Comparison with published laboratory experiments. Continental Shelf Research 28(19): 2668-2677.

## 7 Captions of figures

Figure 01: Hydrodynamic conditions during the simulation of a tidal cycle (both for laboratory experiments and numerical modeling): time series of Kolmogorov microscale  $\eta$  ( $\mu\text{m}$ ) and shear rate  $G$  ( $\text{s}^{-1}$ ) and main stages

Figure 02: Description of floc characteristics assuming floc fractal behaviour: expressions of diameter, volume, density and mass as functions of the primary particle size  $D_p$  and the fractal dimension  $n_f$

Figure 03: Management of the newly formed flocs in the size class distribution: concept of continuous flocculation.

Figure 04: Simulation of the dynamics of the floc population during one tidal cycle: experimental results. Mean floc diameter ( $D$ ) and standard deviation, maximum floc diameter ( $D_{\text{max}}$ ), maximum floc length ( $L_{\text{max}}$ ) and Kolmogorov microscale (minimum  $\eta_{\text{min}}$  and average  $\eta_{\text{mean}}$ ) time series.

Figure 05: Examination of the floc behaviour during the tidal experiment: A : clock-wise hysteresis of the aggregation/fragmentation processes; B: Comparison of the flood and ebb floc size time series (mean floc diameter ( $D$ ), standard deviation and maximum diameter  $D_{\text{max}}$ ).

Figure 06: Time series of floc circularity ( $C$ ) and shear rate ( $G$ ) during the simulated tidal cycle: changes in floc structure.

Figure 07: Comparison between experimental data and model results during the simulated tidal cycle: mean floc diameter (experimental:  $D$ , model:  $D_{\text{mod}}$ ) and maximum diameter (experimental  $D_{\text{max}}$  and model  $D_{\text{max\_mod}}$ ).  $D_{\text{max\_mod}}$  was calculated as the percentile 90.

Figure 08: Floc size distributions time series during a simulated tidal cycle: comparison of model results (upper panel) and experimental data (lower panel). Triangles indicate selected distributions during the tidal cycle for detailed comparison (see Figure 9)

Figure 09: Comparison between observed and computed floc size distributions at given shear rates for aggregation dominant phase (left panel) and fragmentation dominant phase (right panel).

Figure 10: Clock-wise hysteresis of aggregation/ fragmentation processes as simulated with FLOCMOD

Figure 11: Presentation of all size class distribution configurations tested for model optimization: variation of the size range and the number of size classes. The red size class distribution (A.5.4)

corresponds to the optimized parameters, and the blue size class distribution (A.5.1) to the reference size class distribution.

Figure 12: Model sensitivity to the initial distribution: initial distributions shifted upward by 1, 2, 3 or 4 classes from the reference case (upper panel) and related computed mean floc size dynamics (lower panel).

Figure 13: Model sensitivity to floc structural features, i.e. primary particles (upper panel) size and fractal dimension (middle panel) and consequences on mean floc settling velocity (lower panel). Tests with primary particle size  $D_p$  from 2  $\mu\text{m}$  to 10  $\mu\text{m}$  and fixed (1.8, 1.9 and 2.0) or size-dependant fractal dimension ( $n_f$ ) values values.

Figure 14: Model sensitivity related to the influence of floc erosion: role of floc erosion contribution, influence of larger eroded fragments and the number of fragments with three configurations. A: 2 eroded fragments of 9.3  $\mu\text{m}$ , B: 10 eroded fragments of 9.3 $\mu\text{m}$ , C: 2 or 10 eroded fragments of 4  $\mu\text{m}$ .

Figure 15: Consequences of floc erosion contribution to fragmentation: floc size distribution times series with floc erosion contribution of 0% (reference case) (a), 20% (b), 50% (c) and 80% (d). Triangles represent selected periods for detailed investigations (See figure 16)

Figure 16: Consequences of floc erosion contribution to fragmentation: floc size distribution (A and B number distributions, C and D concentration distributions) during slack period (A-C –  $t=400$  min) and high shear rate (B-D –  $t=600$  min)

Figure 17: Floc sizes impacted by collision-induced fragmentation represented by the ratio between collision-induced shear stress and floc strength for three shear rate conditions :  $G=1 \text{ s}^{-1}$  (upper left panel),  $G=5 \text{ s}^{-1}$  (upper right panel) and  $G=10 \text{ s}^{-1}$  (lower left panel)

Figure 18: RMS error between experimental and model results : A for  $\{\alpha, \beta\}$  couples ranging from 0 to 1 and 0 to 0.5 respectively and B for all  $\alpha$  values ranging from 0 to 1 and the corresponding optimal  $\beta$ ; C : comparison and linear relationship between optimal  $\alpha$  and  $\beta$

Table I: Model optimization: influence of the number of size classes (N), upper size limit ( $D_{\text{max}}$ ) on the RMS error and computation time  $t_c$ . Cases A.5.2 to A.5.4 are all based on the same grid size as case A.5.1, but truncated from the corresponding upper and lower limit sizes.

Table II: Floc erosion by shear: test configurations

Figure 1

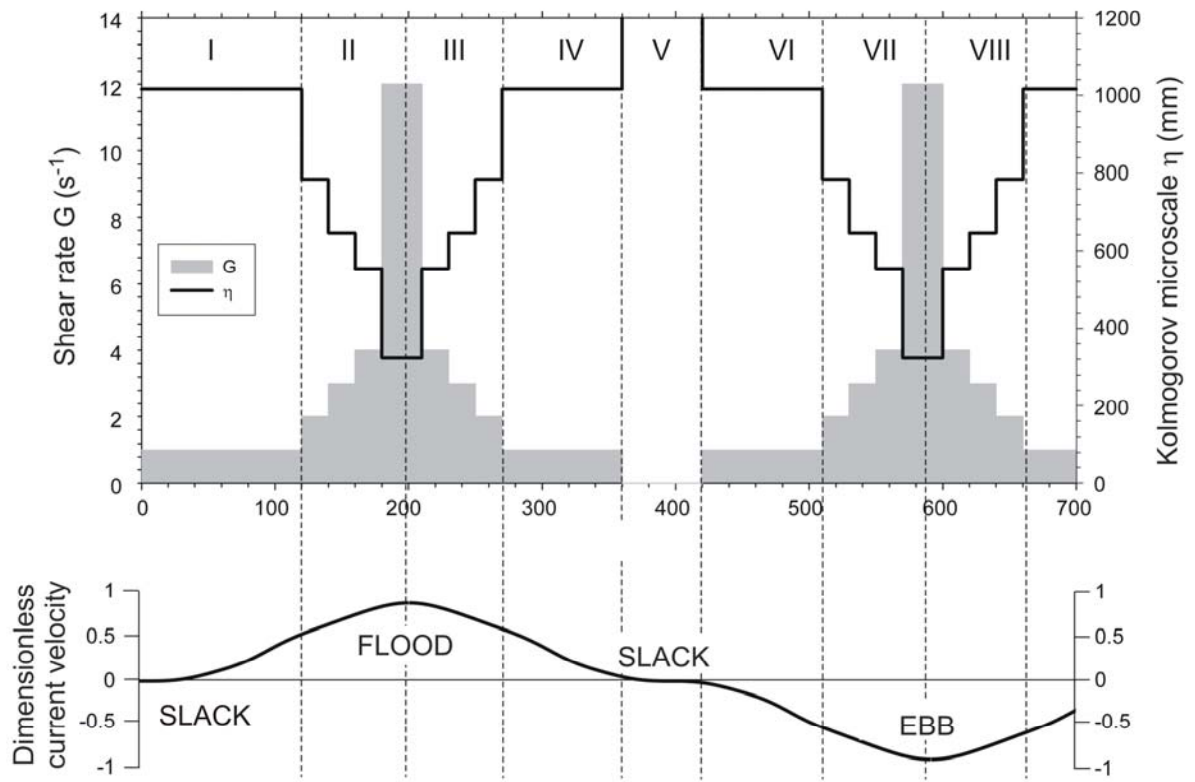


Figure 2

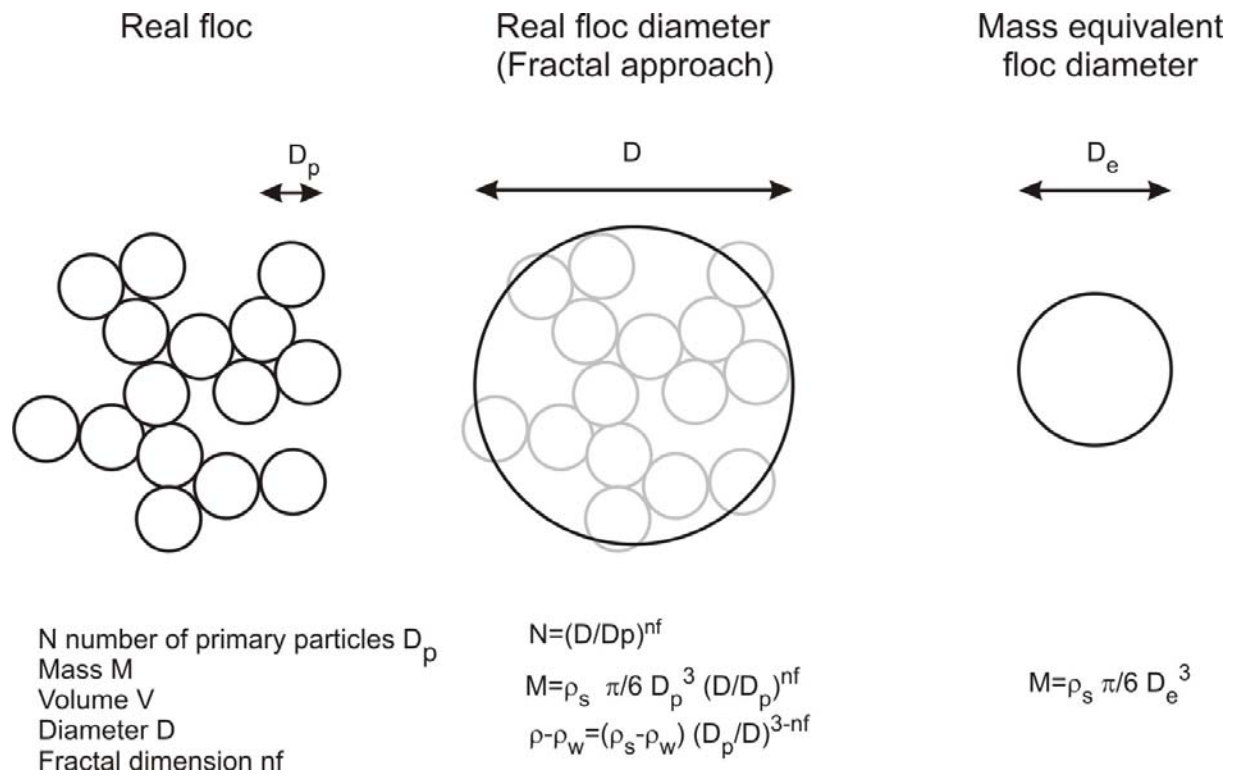


Figure 3

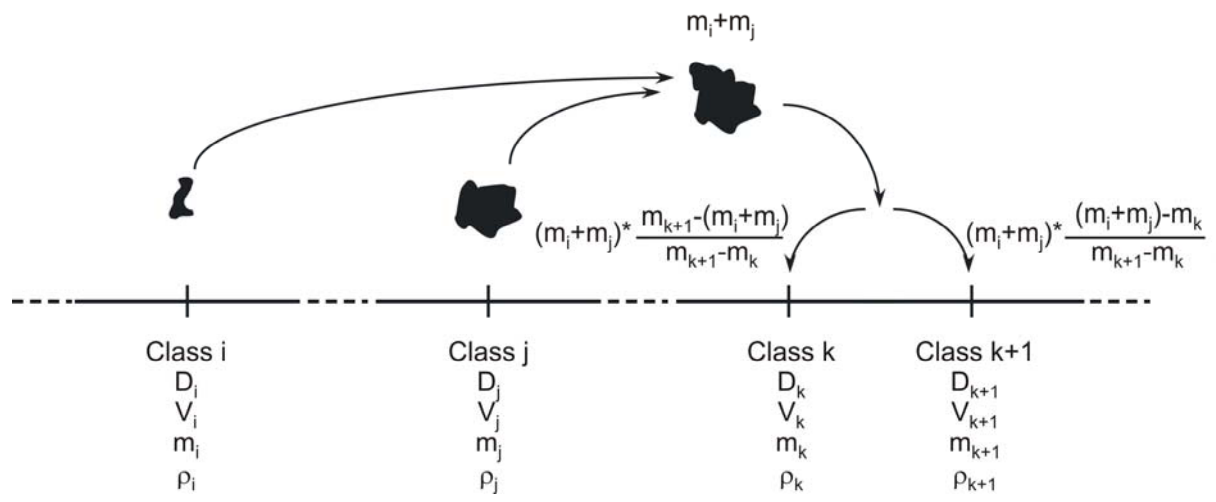


Figure 4

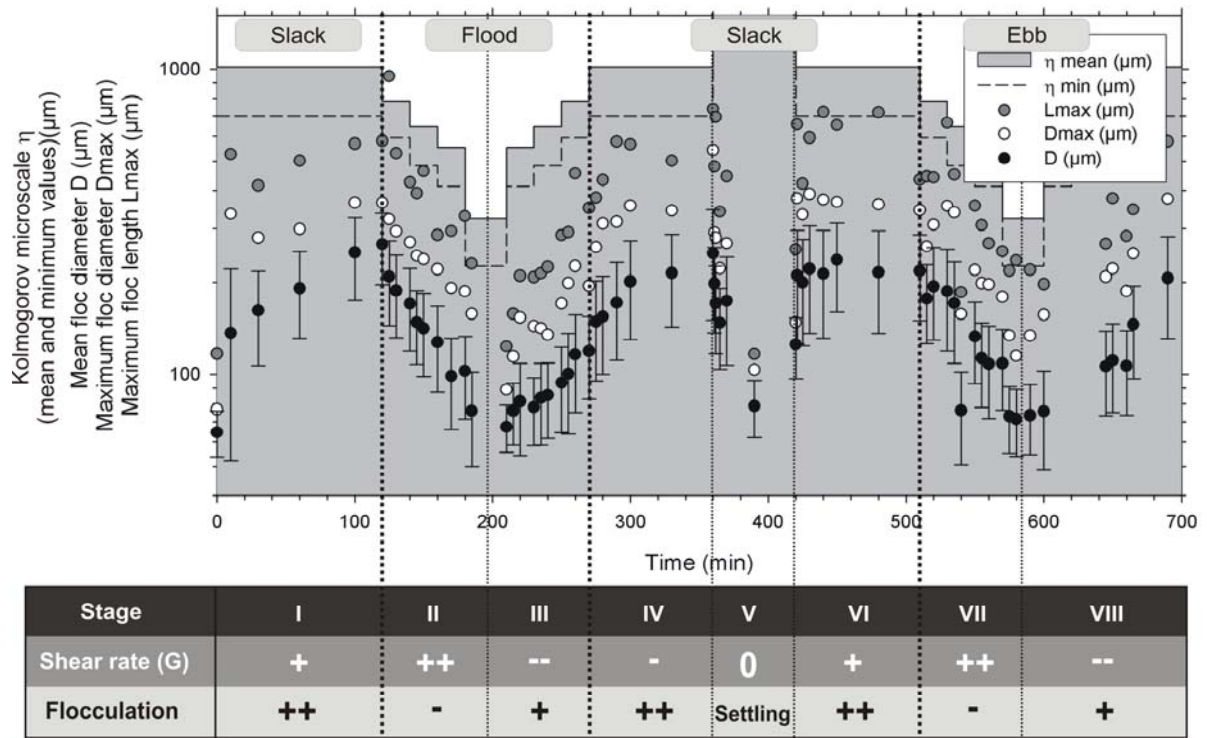


Figure 5

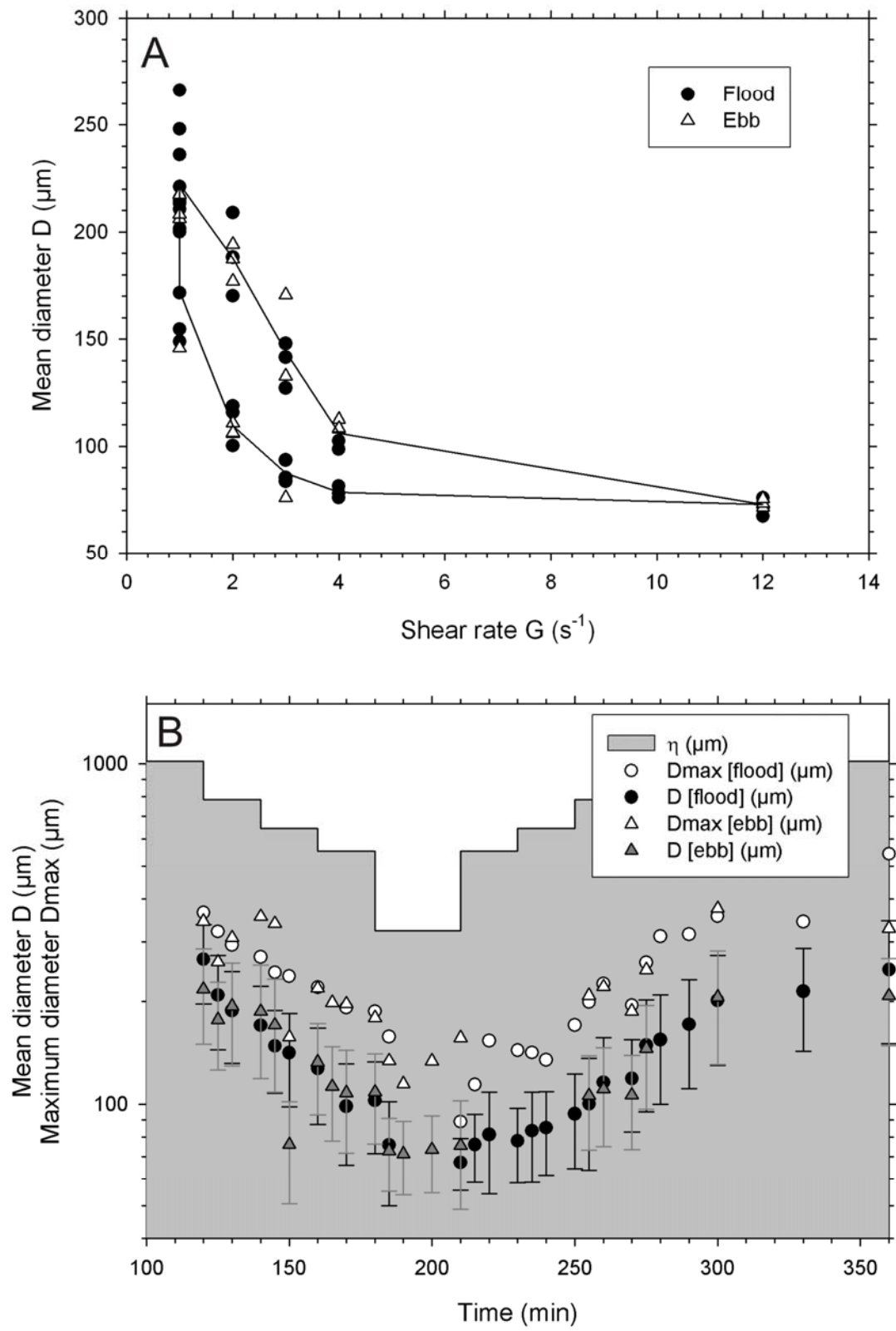


Figure 6

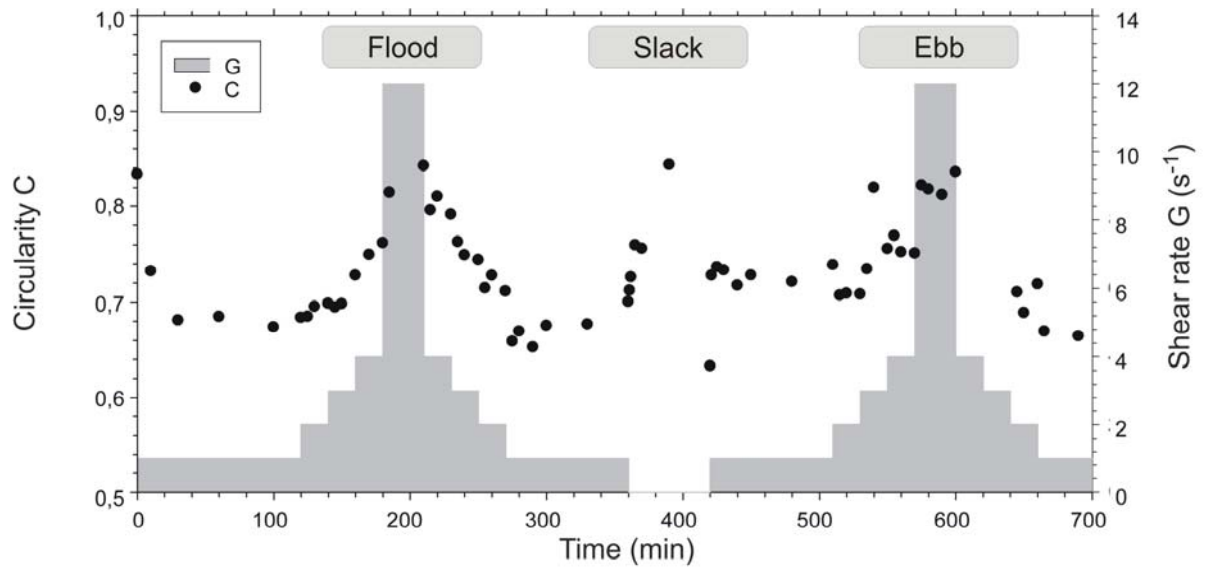


Figure 7

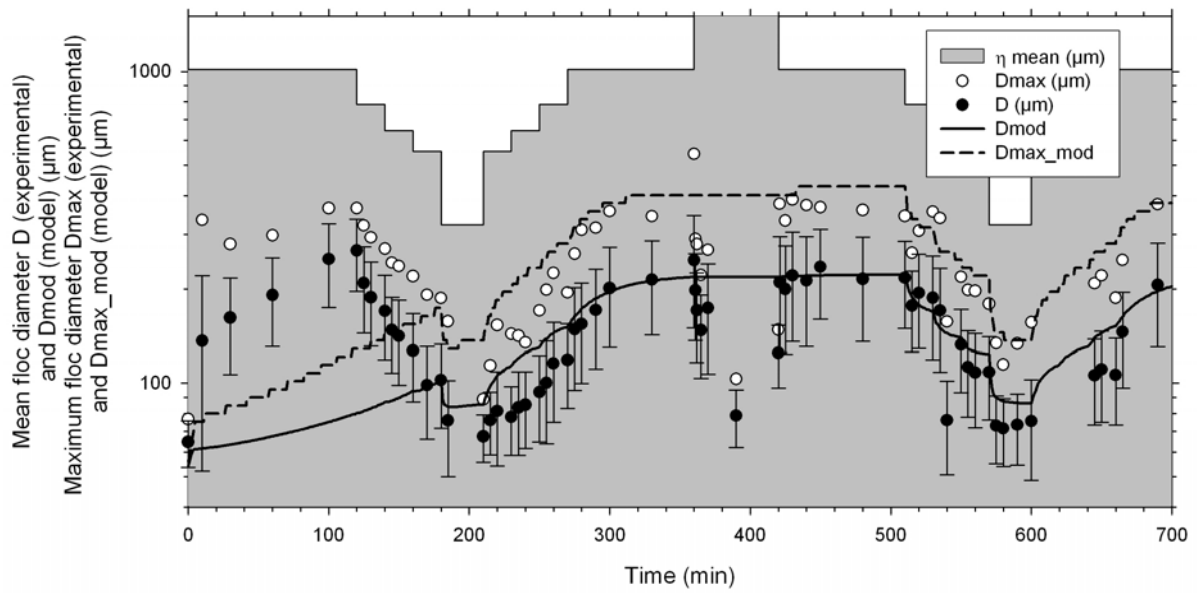


Figure 8

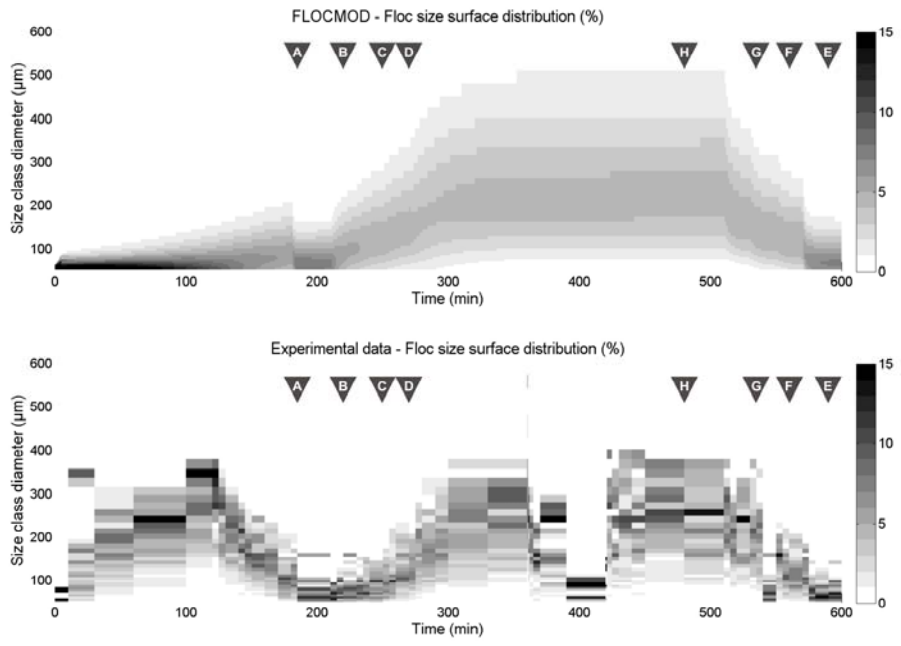


Figure 9

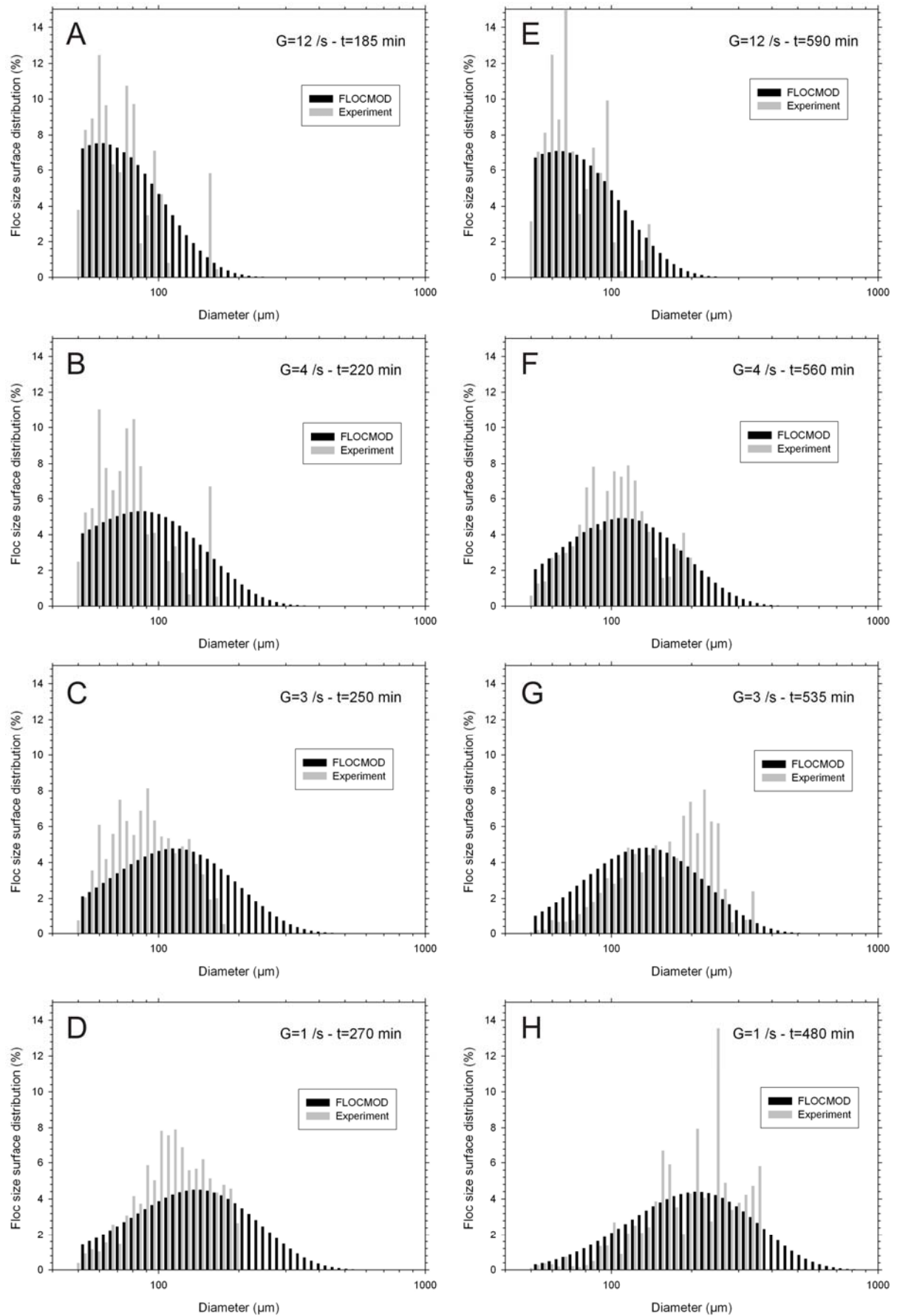


Figure 10

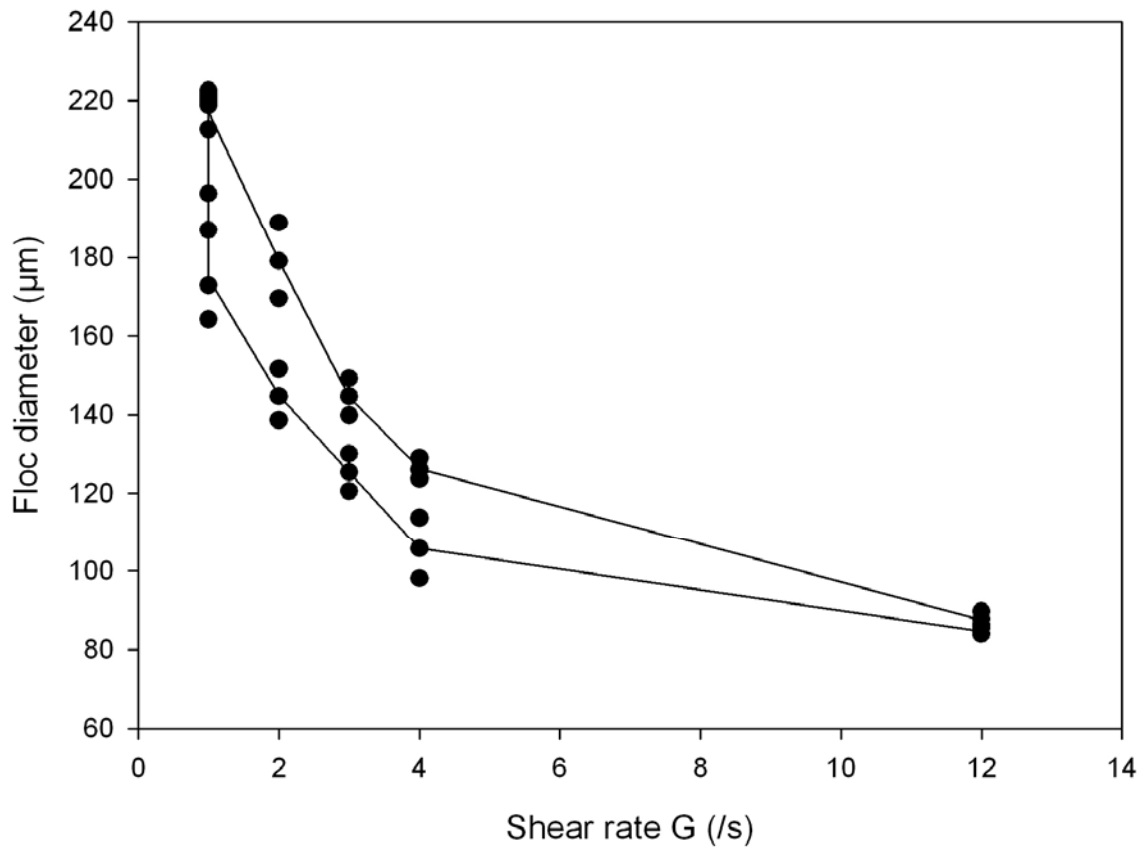


Figure 11

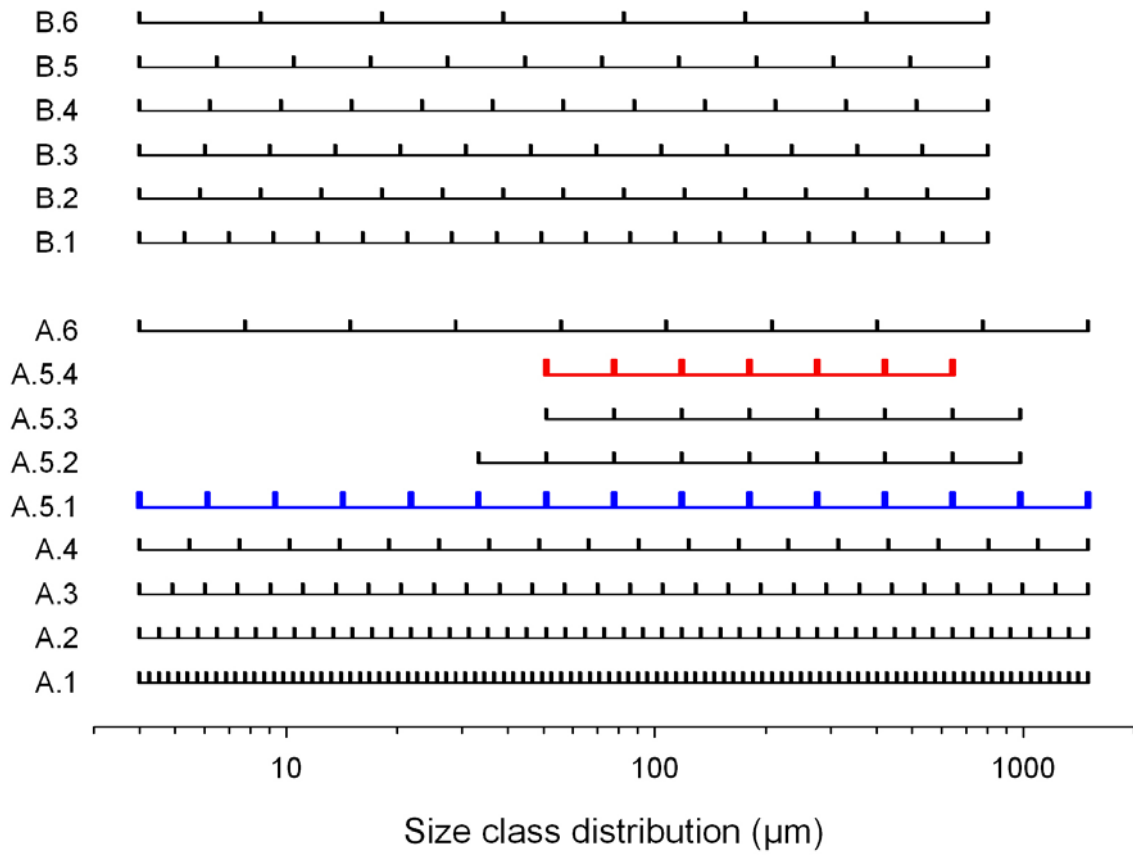


Figure 12

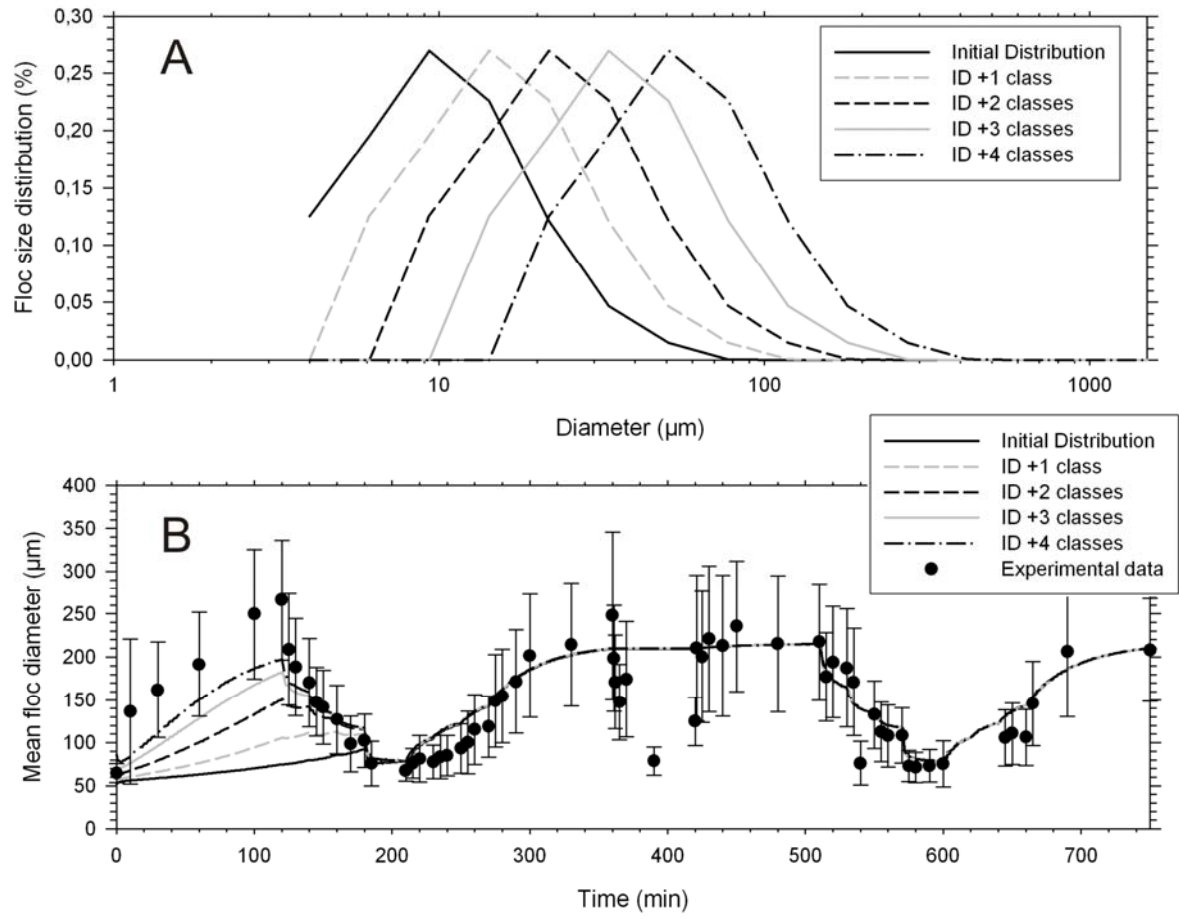


Figure 13

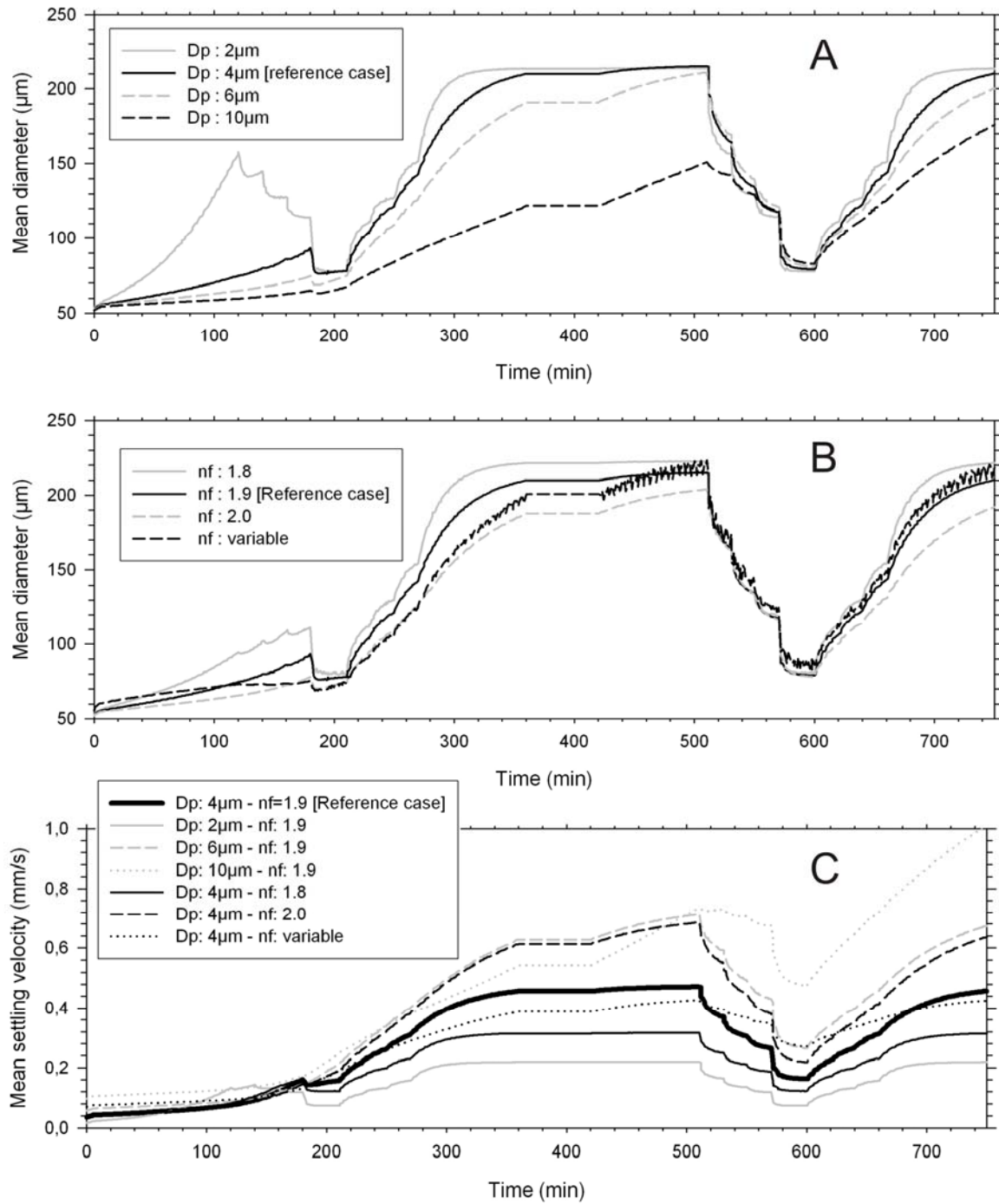


Figure 14

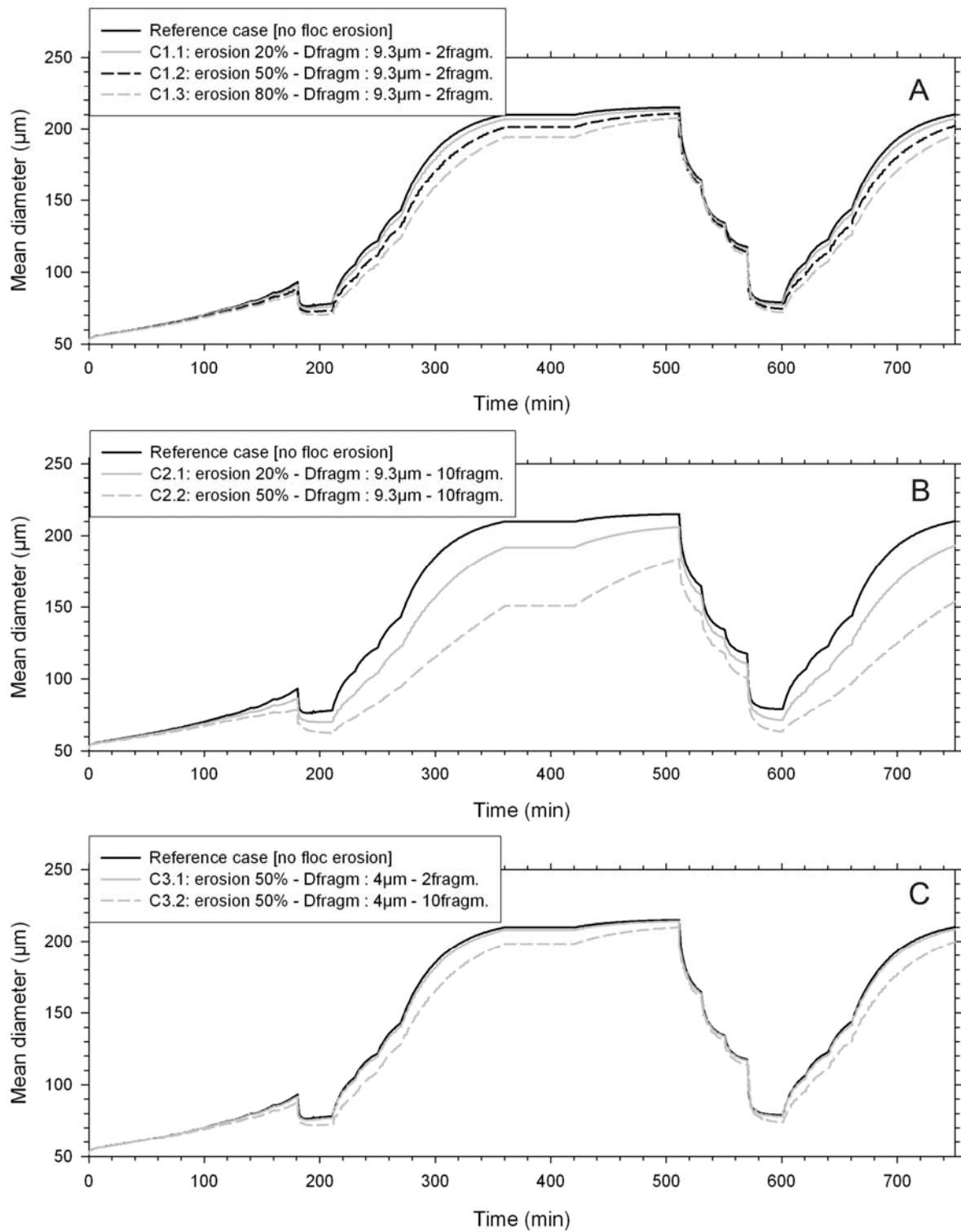


Figure 15

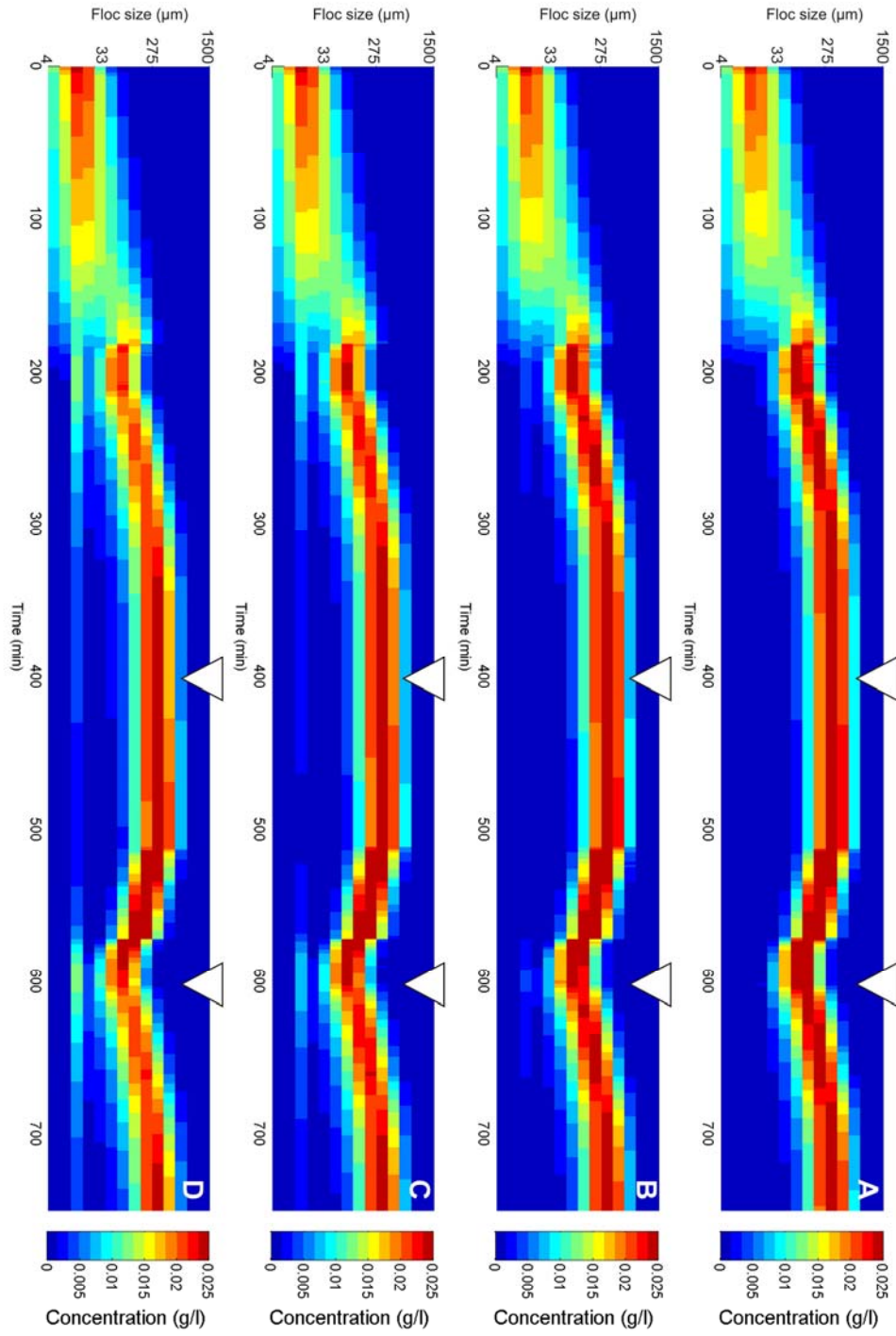


Figure 16

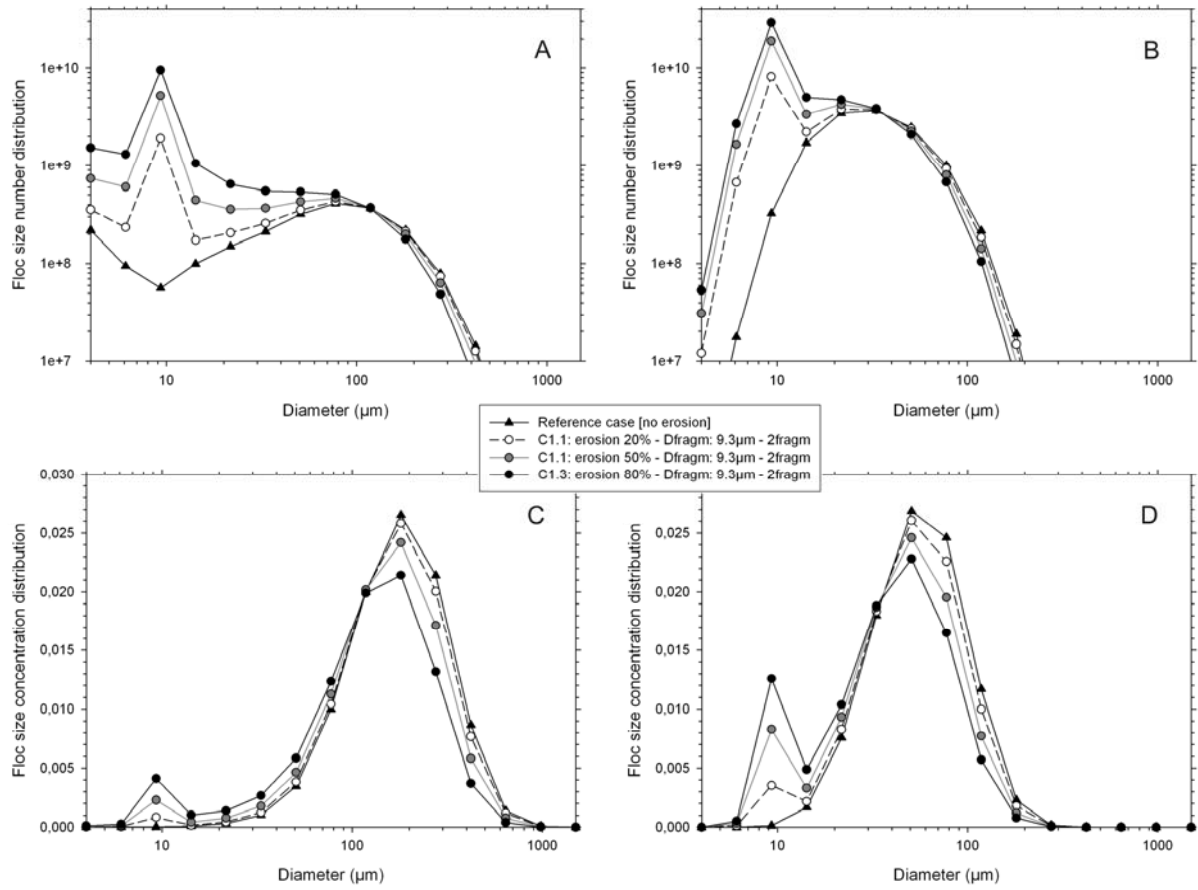


Figure 17

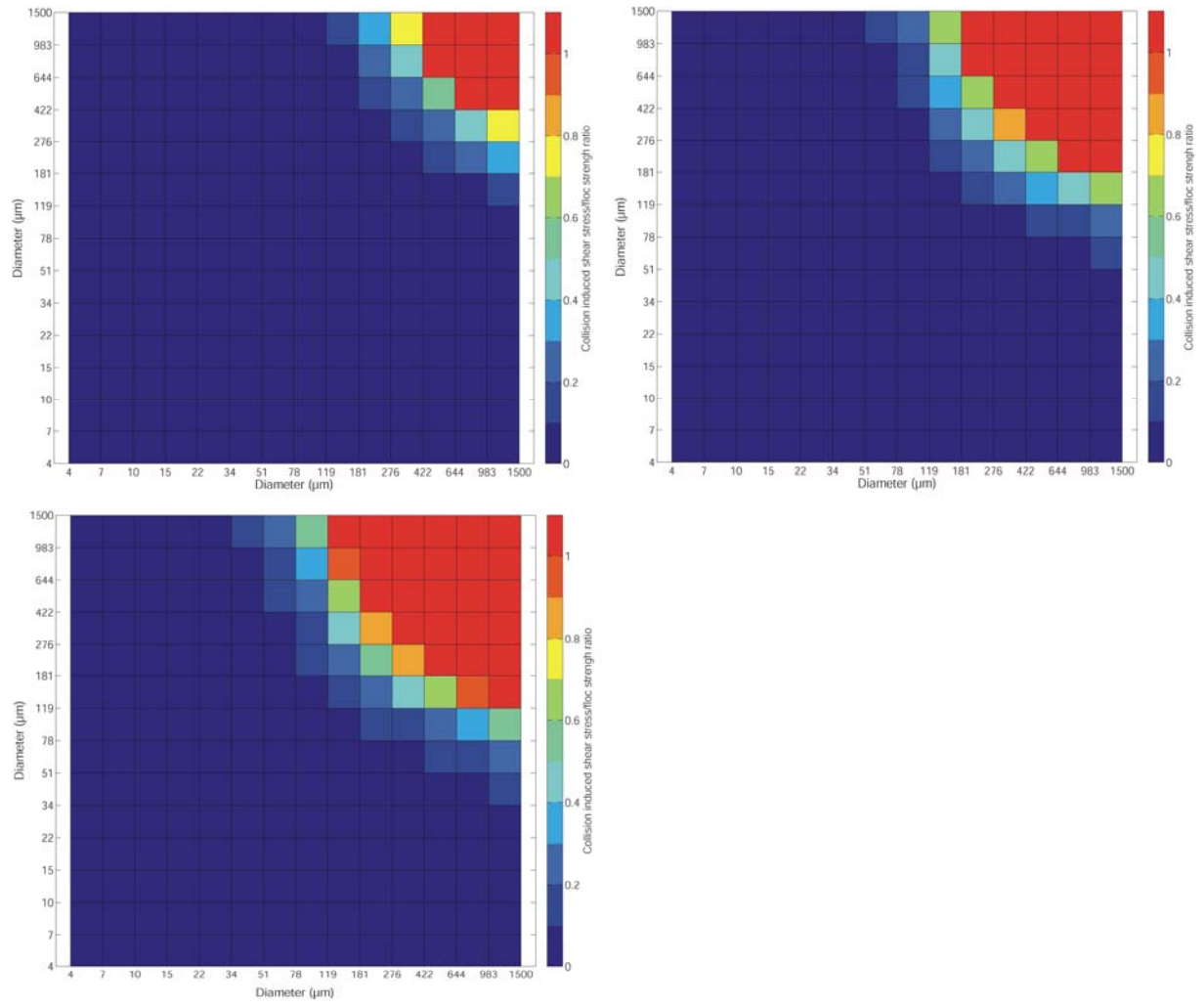


Figure 18

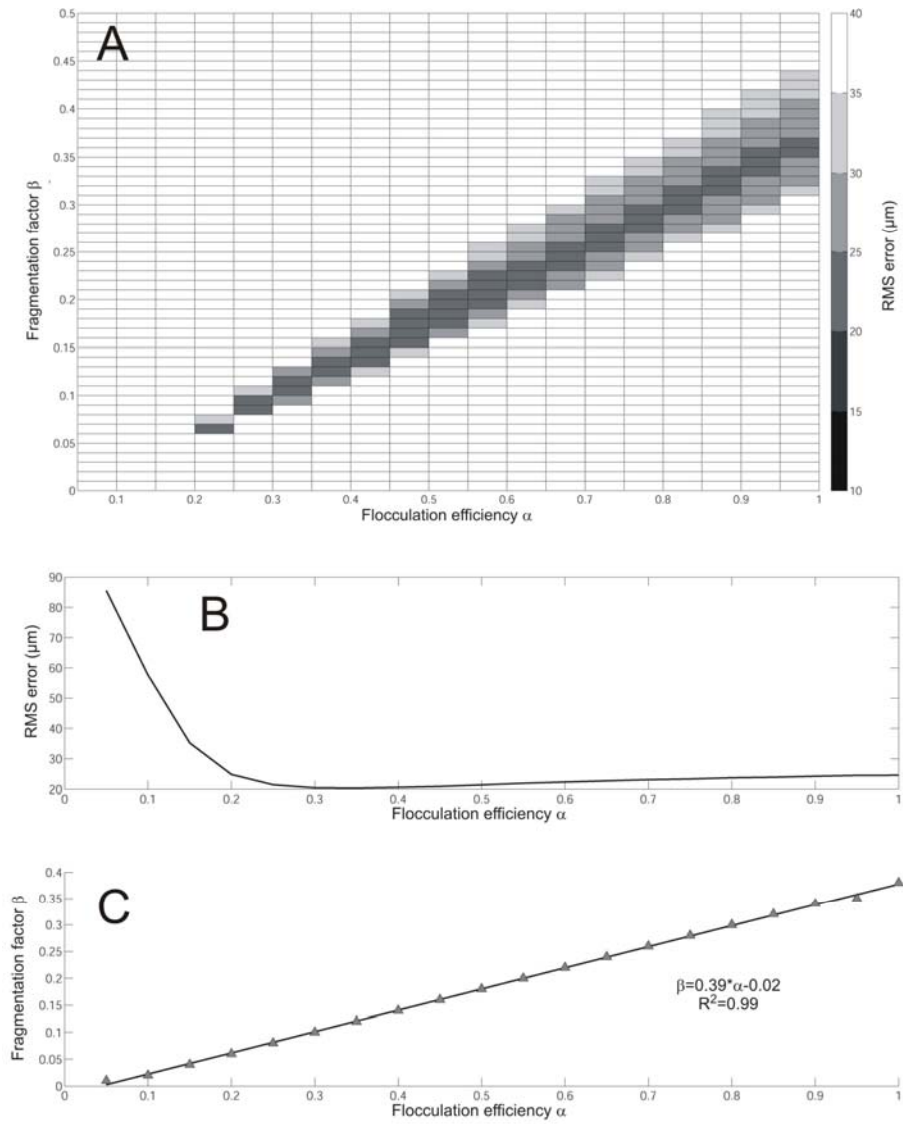


Table I

Case	Number of size classes (N)	Lower size limit (Dmin) in $\mu\text{m}$	Upper size limit (Dmax) in $\mu\text{m}$	RMS Error (ERMS) in $\mu\text{m}$	Computation time (tc) in s
A.1	100	4	1500	0,0	426,0
A.2	50	4	1500	3.0	126,0
A.3	30	4	1500	2.7	49.9
A.4	20	4	1500	2.8	21,0
A.5.1	15	4	1500	8.7	17.2
A.5.2	9	33	982	2.4	7.9
A.5.3	8	50	982	4.8	8,0
A.5.4	7	50	643	4.5	5.6
A.6	10	4	1500	60.3	11.6
B.1	20	4	800	3.3	9.01
B.2	15	4	800	6.1	7.4
B.3	14	4	800	2.8	6.8
B.4	13	4	800	12.2	6.4
B.5	12	4	800	17.8	5.6
B.6	10	4	800	38.6	5.3

Table II

Case	floc erosion contribution	Fragment size [D <sub>fragm</sub> ] (μm)	Number of fragments
C1.1	20%	9.3	2
C1.2	50%	9.3	2
C1.3	80%	9.3	2
C2.1	20%	9.3	10
C2.2	50%	9.3	10
C3.1	50%	4	2
C3.2	50%	4	10